plinary approaches in patients with carcinoma of the esophagus. Chest **113**：S112-S119, 1998
14) 安藤暢敏，石　志紘：食道癌の治療；食道癌の化学療法．日外会誌 **103**：359-363，2002
15) Ilson DH, Kelsen DP：Combined modality therapy in the treatment of esophageal cancer. Semin Oncol **21**：493-507, 1994
16) Ando N, Iizuka T, Ide H, et al：A randomized trial of surgery alone vs surgery plus postoperative chemotherapy with cisplatin and 5-fluorouracil for localized squamous carcinoma of the thoracic esophagus；the Japan Clinical Oncology Group Study (JCOG 9204). Proc Am Soc Clin Oncol **18**：269a, 1999
17) 西尾正道：食道癌の治療；放射線・化学療法．日外会誌 **103**：364-370，2002
18) 西尾正道，堀川よしみ，森田皓三，他：食道癌に対する密封小線源による腔内照射併用の意義．癌の臨 **34**：261-268，1988
19) Okawa T, Tanaka M, Kita M, et al：Superficial esophageal cancer；Multicenter analysis of results of definitive radiation therapy in Japan. Radiology **196**：271-274, 1995
20) Herskovic A, Martz K, Al-Sarraf M, et al：Combined chemotherapy and radiotherapy compared with radiotherapy alone in patients with cancer of the esophagus. N Engl J Med **326**：1593-1598, 1992
21) Murakami M, Kuroda Y, Nakajima T, et al：Comparison between chemoradiation protocol intended for organ preservation and conventional surgery for clinical T1-T2 esophageal carcinoma. Int J Radiat Oncol Bio Phys **45**：277-284, 1999
22) Ohtsu A, Boku N, Muro K, et al：Definitive chemoradiotherapy for T4 and/or M1 lymph node squamous cell carcinoma of the esophagus. J Clin Oncol **17**：2915-2921, 1999
23) Sanyika C：Palliative treatment of esophageal carcinoma, efficacy of plastic versus selfexpandable stents. SAMJ **89**：640-643, 1999
24) Kikuchi M, Nakao M, Inoue Y, et al：Identification of a SART-1 derived peptide capable of inducing the HLA-A24-restricted and tumor-specific cytotoxic T lymphocytes. Int J Cancer **81**：459-466, 1999
25) Uhi T, Yamana H, Sueyoshi S, et al.：Locoregional cellular immunotherapy for patients with advanced esophageal cancer. Clin Cancer Res **6**：4663-4673, 2000
26) 谷川啓司，清水公一，藤沢俊美，他：第2世代樹状細胞（DC）局注療法の臨床研究．Biotherapy **15**：54，2001
27) Shimada H, Shimizu T, Shiratori T, et al：Preclinical study of p53 gene therapy for esophageal carcinoma. Surgery Today **31**：597-604, 2001

(KITAGAWA Yuko, et al 慶應義塾大学医学部外科：〒160-8582 東京都新宿区信濃町 35)

日外会誌　103（12）：865～868，2002

特　集

術後感染症対策の最近の進歩と問題点

5．食道外科領域における術後感染症

慶應義塾大学医学部外科

小澤　壯治，北川　雄光，岡本　信彦，清水　芳政，北島　政樹

キーワード　食道癌，術後感染症，MRSA，予測，自己血輸血

I．内容要旨

食道外科領域とくに食道癌術後感染症を中心に解説した．食道癌術後感染症のうち「術野感染」である創感染の頻度は低く，むしろ「術野外感染」である肺炎の頻度が高い．術後感染症の発症を阻止する目的で投与する「術後感染発症阻止薬」と，術後感染の治療目的で投与する「術後感染治療薬」を区別する考え方が重要である．

術後感染症発症を予測する試みとして，phytohemagglutinin（PHA）と concanavalin A（Con A）刺激による末梢血単核球の増殖能から術前の細胞性免疫能を調べる方法や，術後2時間目の白血球数や第1病日の白血球数の減少に注目する方法がある．さらに術後MRSA感染症発症は術前の血清IgG2値低下で予測できる．

治療に関する進歩を以下に挙げる．MRSA感染症発症率を低下させるためには，MRSAに抗菌力のある鼻腔用ムピロシン軟膏（mupirocin calcium hydrate）を術前に使用する．術後免疫力低下を避けるために，輸血が必要ならば同種血輸血を避け自己血輸血を行う．術後肺炎発症を防止するためには，術前化学放射線療法の照射線量は40Gy以下に抑える．

II．はじめに

本邦において食道疾患に対する外科治療の大部分を食道癌手術が占める．食道癌手術は頸部，胸部，腹部の3領域に手術操作が及ぶため，消化器外科手術の中で侵襲が大きいと考えられている．また，近年の集学的治療法の進歩に伴い術前に化学療法，放射線療法，化学放射線療法を受けている患者も増えてきたため，周術期の病態が複雑になってきた．本稿では食道外科領域とくに食道癌術後感染症を中心に最近の進歩と問題点を解説する．

III．食道癌術後感染症の特徴

食道癌手術では食道を切離する操作と再建胃管や再建結腸を作成して吻合する操作以外は消化管が開放されたり断端が生じることはなく，術中汚染の機会は少ない．そのため「術野感染」である創感染の頻度は3.4%～4.8%と低く，むしろ「術野外感染」である肺炎の頻度は18.8%～24.2%と高い[1][2]．術後感染症は，38.5℃以上の発熱，白血球数4,000/uL以下または10,000/uL以上，炎症巣または菌血症，これら3項目すべてが認められる病態とし，肺炎は胸部単純X線写真による異常陰影および喀痰の細菌培養陽性が認められる病態とすると理解しやすい[3]．

IV．術後感染症の対策と予測

食道癌手術では術後感染症の中でも肺炎の発症頻度が高く，術後予防的抗菌薬投与の際には抗菌スペクトルの広い薬剤や多剤の長期間投与が一般的であった．最近では多剤耐性菌出現などの問題から抗菌スペクトルの狭い薬剤を短期間投与することが必要とされてきた．具体的には術後感染症の発症を阻止する目的で投与する「術後感染発症阻止薬」と，術後感染の治療目的で投与する「術後感染治療薬」を区別する考え方が

INFECTIOUS COMPLICATIONS AFTER ESOPHAGEAL SURGERY
Soji Ozawa, Yuko Kitagawa, Nobuhiko Okamoto, Yoshimasa Shimizu and Masaki Kitajima
Department of Surgery, School of Medicine, Keio University, Tokyo, Japan

重要とされている[4]．「術後感染発症阻止薬」としては食道内細菌はグラム陽性菌が75%を占めていることから，第一世代セフェム（CEZなど）やペニシリンが適当であり，一方「術後感染治療薬」としては，再建胃管内ではグラム陰性桿菌が62%占め，さらに術後喀痰培養検出菌の71%がグラム陰性桿菌であることから，グラム陰性桿菌を標的とした第3.5世代セフェム(CZOP, CPRなど）やカルバペネム系抗菌薬を推奨する報告があり参考になる[2]．

術後感染症発症を予測する研究が進められている．Takagiらは術前の免疫能に注目して103例の食道癌症例を対象に術後感染予測を検討した[5]．すなわちphytohemagglutinin (PHA) とconcanavalin A (Con A) 刺激による末梢血単核球の増殖能を術後感染群と非感染群と比較したところ，術後感染群では術前にすでに増殖能が低下していたことを見い出した．したがって，術前の細胞性免疫能を調べることにより，術後感染症の発症リスクが高い症例を予測することが可能になった．

また樽井らは32例の食道癌症例について解析し，肺炎，膿胸，上縦隔炎，腹腔内膿瘍などの術後重症感染症は37.5%に発症し，非感染症例に比べて術後2時間目の白血球数が少なく，第1病日の白血球数の減少が有意に低値を示すことを明らかにした[6]．さらに抗炎症性サイトカインIL-10と炎症性サイトカインIL-6，G-CSFの比は術後2時間目と術後1日目に感染症群で有意に低値であることも示した．術後感染症発症率と術後早期の臨床検査データーとの関連を解析すると，Δ白血球数，IL-6，G-CSF，IL-10/IL-6，IL-10/G-CSF，直腸pHiが術後感染症リスク判定に有用であると報告している．これは術直後の検査値を注意深く評価することで可能なリスク判定であり，利用価値が高い．

Nakamuraらも術後1週間に白血球数が術前値の150%以上に上昇しない症例では肺炎を発症しやすく，それは肺への白血球集積が原因と報告している[7]．

V. MRSA感染症の予測，対策，治療

1980年代後半から問題となったメチシリン耐性黄色ブドウ球菌（MRSA）感染症は，効果的な抗菌薬の使用や院内感染対策の充実によりその感染頻度が減少してきた．最近ではその頻度は1.9～2.9%と低い[8][9]．しかし，手術侵襲の大きな食道癌手術後には喀痰喀出力や免疫力の低下などにより感染準備状態にあり，MRSA感染症は最も注意するべき院内感染症である．

MRSA感染対策の一環として，易感染者の予測が必要である．齊藤貴生らは，術前の感染防御能の異常と術後MRSA感染症発症との関連について検討した[10]．術後MRSA感染症例では非感染例に比し，術前の抗PPS-IgG値（pneumococcal polysaccaride (PPS) に対する特異抗体産生能）が低下していることを報告した．これは，肺炎球菌ワクチンで患者を免疫し，2～3週後に採血後，血清中の抗PPS-IgGをELISA法で測定する．また，IgGサブクラスの中で血清IgG2値が低下している症例も術後MRSA発症を起こしやすいこと，抗PPS-IgGと血清IgG2値が相関することを明らかにし，ルチーン検査として血清IgG2値の低下を評価することにより術後MRSA感染発症を予測する可能性を示した．

齊藤礼次郎らの食道癌272例の検討では，MRSA検出率は17.6%で，MRSA感染症として肺炎，膿胸，創感染などが多く，術後早期の感染，術後合併症発症，複数菌感染などが特徴としている[11]．その実態から，術後早期での徹底した院内感染対策，適切な手術適応および手術操作による術後合併症の回避が重要と述べている．

注目するべき対策として，田中らはMRSAに抗菌力のある鼻腔用ムピロシン軟膏（mupirocin calcium hydrate）を術前に使用することの有用性を報告した[8]．ムピロシン軟膏を術前1日3回，3日間鼻前庭部に左右それぞれ30mgずつ塗布し，MRSA検出率を対照群の19.1%から3.7%まで減少させ，さらにMRSA感染症発症率は1.85%におさえることに成功した．病院内にはMRSA保菌患者が確実に存在することから，鼻腔内のMRSA治療を術前に行うことの有用性を報告した．複数回使用による耐性株の出現に注意は必要で，術前の単回使用を推奨している．

別の試みとして，岩田らは術後MRSA腸炎予防における希塩酸注入法を検討した[12]．MRSAが酸に弱耐性であり，MRSA腸炎の多くが食道癌，胃癌の術後に発症し，胃酸分泌機能の喪失がMRSA腸炎の発症要因と考え，動物実験を行った．MRSAに対して殺菌効果を発現するのはpH 2.5以下であり，pH 2.0で30分間，pH 1.5で5分間の接触で99%以上の発育阻止を認めた．食道癌患者に対してはpH 2の希塩酸20～40mLを排ガス後の胃ゾンデ抜去まで施行した．MRSA検出率は非注入群33.3%から注入群4.8%，術後腸炎発症率は非注入群28.6%から注入群4.8%，いずれも希塩酸注入群で低下してMRSA腸炎予防における希塩酸注入法の有用性を報告している．術後の上部消化管を酸性環境にする

術後管理は独創的で有望であるが，胃管内へ注入された希塩酸によるびらんや潰瘍発症についての慎重な観察が必要である．

VI. 自己血輸血と感染症

平成11年度の厚生労働省の赤血球製剤使用状況調査によれば，食道癌手術では約46%の症例で術中輸血が施行されている[13]．一方で，周術期の同種血輸血が免疫能を抑制し，術後感染症の増加を引き起こすという報告がある．食道癌手術でも自己血輸血は可能であるが，調査によれば自己血輸血を実施している施設は23%にすぎない．同種血輸血の術後感染症へ及ぼす影響について興味深い研究がある．

木ノ下らは年齢80歳以下，体重40kg以上，術前Hb 11.0g/dL以上，術前TP 6.5g/dL以上，術前高度の合併症を有しない症例を自己血輸血プログラムの対象として，手術予定2週間前までに400mLの採血を行い凍結保存し，手術予定1週間前にHb 12.0g/dL以上あれば第2回目の自己血400mLを採血し，液状保存している．348例を対象とした検討によれば，術後感染症発症率は自己血輸血群で同種血輸血を受けなかった症例で11.3%，同種血輸血を受けた症例で26.8%，肺炎の発症率もそれぞれ8.2%，20.7%と自己血輸血に比べて同種血輸血は術後感染症発症に強く関わっていた[3]．したがって輸血が必要な際には自己血輸血が望ましいと述べている．同時に多変量解析による術後感染症発症予測を行っているが，同種血輸血施行例，腫瘍占居部位が気管分岐部より上の症例，8時間以上の手術時間の3因子を危険予測因子としている．このように同種血輸血が術後感染症の増悪因子とするならば，対策として第1に輸血を必要としない手術法を選択すること，第2に出血や貧血に対する輸血の基準を厳密にすること，第3に輸血が必要なら同種血輸血を避け自己血輸血を行うことを薦めている．

VII. 術前治療と感染症

食道癌に対する集学的治療が盛んに行われるようになり，術前に化学療法や化学放射線療法を受け，手術に臨む症例が増加してきた．教室での検討によると化学放射線療法施行症例では一度減少した白血球数は約70%まで回復するが，手術侵襲によっても治療前値以上に平均値は増加することなく術後1カ月間推移した[14]．これはリンパ球数や血小板数でも同様であり，化学放射線療法がもたらす骨髄抑制状態が少なくとも術後1カ月以上は遷延していることを示していた．したがって，術前治療を受けた症例では術後感染に通常手術以上に注意する必要がある．

Eguchiらは化学放射線療法と術後合併症の検討を行った[15]．5-FUとCDDPによる化学療法と放射線療法を術前に施行した場合，照射線量が60Gy以上では術後肺炎が67%発症し，それは照射線量40Gy以下に比べて有意に高率であり，術前化学放射線療法の照射線量は40Gy以下に抑える必要があると述べている．術前補助療法を行う際に，術後肺炎発症の観点から照射線量を制限する必要性を強調した点で評価できる．

VIII. おわりに

食道癌術後感染症は周術期管理の進歩により減少しつつある．今後は，簡便で信頼性の高い感染症発症予測法の開発，クリニカルパスを導入した周術期管理の質の向上，適切な手術適応の設定，術前治療後の特殊周術期管理法の確立などが課題として挙げられる．20世紀には手術が食道癌治療の主役であったが，21世紀となり他の治療手段が台頭して手術の位置づけが不明確になるおそれがある．しかし，食道癌術後合併症のうち感染症を克服して手術成績を向上させることは，外科治療の意義を明確にするうえで非常に重要なことである．

文　献

1) 溝手博義，疋田茂樹，吉田祥吾，他：食道癌患者の術後感染症対策．癌と化学療法，19：167—172，1992.
2) 斉藤礼次郎，本山悟，奥山　学，他：食道癌手術における予防的抗菌薬投与法．外科，63：143—147，2001.
3) 木ノ下義宏，宇田川晴司，鶴丸昌彦，他：食道癌手術における自己血輸血．Prog Med，20：254—259，2000.
4) 炭山嘉伸，草地信也：術後感染発症阻止薬の基本的な考え方．消化器外科，23：277—281，2000.
5) Takagi K, Yamamori H, Morishima Y, et al.: Preoperative immunosuppressionits relationship with high morbidity and mortality in patients receiving thoracic esophagectomy. Nutrition：13—17，2001.
6) 樽井武彦，金　成弼，辻仲利政，他：食道癌根治術における術後感染症の発症予測に関する検討．日本外科感染症研究，10：4—9，1998.
7) Nakamura E, Ando N, Ozawa S, et al:Post-operative changes in leucocytes and pulmonary complications following esophageal cancer surgery. The Proceedings of XXX World Congress of the International College of Surgeon. 267—271, Monduzzi Editore, 1996.
8) 田仲　曜，島田英雄，千野　修，他：食道癌手術に

おけるムピロシン軟膏の有用性．日消外会誌，33：567—571, 2000.
9) 草地信也，炭山嘉伸，碓井貞仁，他：食道癌術後MRSA感染の予防対策と効果．日臨外会誌，57：2076—2077, 1996.
10) 斎藤貴生，木下忠彦，重光祐司，他：食道癌術後MRSA感染とその対策—特に易感染者の術前予知について．日外会誌，93：895—897, 1992.
11) 斉藤礼次郎，阿保七三郎，北村道彦：食道癌術後MRSA感染とその対策．日臨外会誌，57：2615—2622, 1996.
12) 岩田尚士，山下芳典，高島郁博，他：術後MRSA腸炎予防における希塩酸注入法に関する実験的ならびに臨床的研究．日臨外会誌，55：3018—3022, 1994.
13) 小澤壯治，久保正二，高橋慶一，他：食道悪性腫瘍手術における赤血球製剤使用状況調査．日臨外会誌，63（増刊号）：481, 2002.
14) 小澤壯治，安藤暢敏，北島政樹：化学放射線療法．消化器科，25：154—160, 1997.
15) Eguchi R, Ide H, Nakamura T, et al.: Analysis of postoperative complications after esophagectomy for esophageal cancer in patients receiving neoadjuvant therapy. Jpn J Thorac Cardiovasc Surg, 47：552—558, 1999.

INFECTIOUS COMPLICATIONS AFTER ESOPHAGEAL SURGERY

Soji Ozawa, Yuko Kitagawa, Nobuhiko Okamoto, Yoshimasa Shimizu and Masaki Kitajima
Department of Surgery, School of Medicine, Keio University, Tokyo, Japan

The incidence of wound infection, which is an intrasurgical field infection, is lower than the incidence of pneumonia, which is an extrasurgical field infection, after esophageal cancer surgery. Several trials predicting postoperative infectious complications have been reported. One measured the phytohemagglutinin- and concanavalin A-induced proliferation of peripheral blood mononuclear cells in patients ; one measured the white blood cell (WBC) count 2 h after surgery and the decrease in WBC count on first postoperative day ; and another showed that the decrease in serum IgG_2 level can predict the occurrence of methicillin-resistant *Staphylococcus aureus* (MRSA) infections. Useful strategies for managing infectious complications have also been reported. Applying mupirocin calcium hydrate ointment to the nasal cavity decreases the incidence of MRSA infections. Autologous blood collection reduces the need for allogeneic transfusion in patients undergoing resection of esophageal cancer, and avoidance of allogeneic transfusion may reduce the risk of postoperative infection. The total exposure to preoperative chemoradiotherapy should be limited to 40 Gy or less to prevent postoperative pneumonia.

Heterozygosity with respect to *Zfp148* causes complete loss of fetal germ cells during mouse embryogenesis

Akihide Takeuchi[1,3], Yuji Mishina[2], Osamu Miyaishi[1,3], Eiji Kojima[1], Tadao Hasegawa[1,3] & Ken-ichi Isobe[1]

Published online 13 January 2003; doi:10.1038/ng1072

Zfp148 belongs to a large family of C2H2-type zinc-finger transcription factors. Zfp148 is expressed in fetal germ cells in 13.5-d-old (E13.5) mouse embryos. Germ-line transmission of mutations were not observed in chimeric *Zfp148*$^{+/-}$ mice, and some of these mice completely lacked spermatogonia. The number of primordial germ cells in *Zfp148*$^{+/-}$ tetraploid embryos was normal until E11.5, but declined from E11.5 to E13.5 and continued to decline until few germ cells were present at E18.5. This phenotype was not rescued by wild-type Sertoli or stromal cells, and is therefore a cell-autonomous phenotype. These results indicate that two functional alleles of *Zfp148* are required for the normal development of fetal germ cells. Recent studies have shown that Zfp148 activates p53, which has an important role in cell-cycle regulation[1]. Primordial germ cells stop proliferating at approximately E13.5, which correlates with induction of phosphorylation of p53 and its translocation to the nucleus. Phosphorylation of p53 is impaired in *Zfp148*$^{+/-}$ embryonic stem cells and in fetal germ cells from chimeric *Zfp148*$^{+/-}$ embryos. Thus, *Zfp148* may be required for regulating p53 in the development of germ cells.

Zfp148 (also known as *BFCOL-1*, *ZBP-89*, *BERF1* and *ZNF148*) encodes a Krüppel-type transcription factor of 89 kD with four tandem zinc-finger DNA-binding motifs[2,3]. Zfp148 is thought to promote growth arrest by stabilizing p53. Zbp-89, a rat homolog of Zfp148, enhances p53 transcriptional activity and prevents degradation by binding to p53 through its zinc-finger domain[1]. Overexpression of Zbp-89 leads to accumulation of p53 in the nucleus, activation of $p21^{waf1}$ and cell-cycle arrest. Zfp148 also interacts with growth-arrest DNA damage-34 (Gadd34; ref. 3) and activates the *Cdkn1a* promoter[4]. These activities suggest that Zfp148 has an important role in regulating cellular proliferation; it may also be important during development.

Zfp148 is highly expressed in the neural tube (A.T., Y.M., O.M. and K.-I.I., unpublished observations) and in male and female

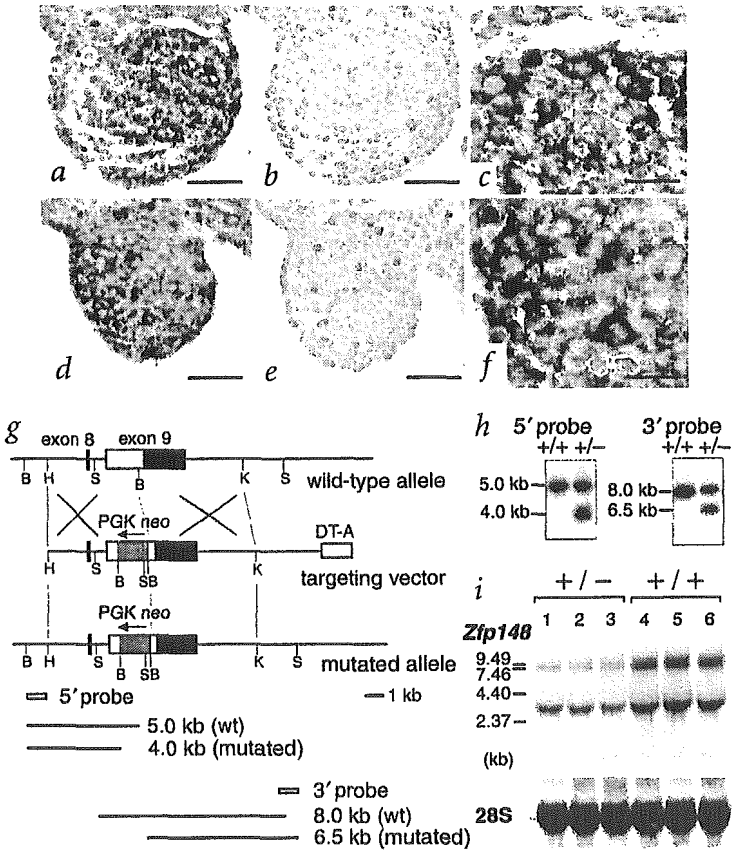

Fig. 1 *In situ* hybridization of male and female gonads of E12.5 embryos and targeted disruption of *Zfp148*. *a–f*, *In situ* hybridization of male (*a–c*) and female (*d–f*) gonads with antisense (*a,c,d,f*) and sense (*b,e*) RNA probes specific to *Zfp148*. Positive signal (violet granules) was detected in the genital ridge in male and female gonads. The positive signal was detected in the tubular structure of the male gonads (*a*) but in the peripheral area of the female gonads (*d*). At higher magnification, the positive signal was detected predominantly in PGCs, large cells with large nuclei (*c,f*). No signal was detected with the sense probe (*b,e*). Scale bar = 100 μm (*a,b,d,e*) or 50 μm (*c,f*). *g*, Construction of the *Zfp148* targeting construct. Non-coding region is shown as a black rectangle in exon 9. Unique 5′ and 3′ probes are shown as open boxes. B, *Bam*HI; H, *Hin*dIII; K, *Kpn*I; S, *Spe*I; DT-A, diphtheria toxin A. *h*, Southern-blot analysis using indicated probes. ES-cell DNA digested with *Bam*HI produces bands of 5.0 kb (wild-type) or 4.0 kb (mutated allele) with the 5′ probe, and ES-cell DNA digested with *Spe*I produces bands of 8.0 kb (wild-type) or 6.5 kb (mutated allele) band with the 3′ probe. *i*, Northern-blot analysis of the targeted and non-targeted ES clones. Lanes 1–3 are targeted clones generating infertile chimeric mice (clone 011, 013 and 014, respectively). Lanes 4–6 are control non-targeted clones from the same screening (clone 021, 023 and 025, respectively). All non-targeted clones showed germ-line transmission. *Zfp148* mRNA is detected as three species in Northern blots[2,24,25]. Expression of all three species was 50% lower in the heterozygous mutant ES cells than in control ES cells (52.8% for two upper bands and 45.1% for the bottom band) when hybridized with any *Zfp148* probes except that for exon 9. Blots were hybridized with a probe for 28S ribosomal RNA probe to confirm equal sample loading.

[1]*Department of Basic Gerontology, National Institute for Longevity Sciences, 36-3 Gengo, Morioka-cho, Obu-city, Aichi 474-8522, Japan.* [2]*Molecular Developmental Biology Group, Laboratory of Reproductive and Developmental Toxicology, National Institute of Environmental Health Sciences/National Institutes of Health, Research Triangle Park, North Carolina, USA.* [3]*Present addresses: Neural Stem Cell Research, Stem Cells Inc., 3155 Porter Drive, Palo Alto, California 94304, USA (A.T.); Department of Pathology, Aichi Medical University School of Medicine, Nagakute, Aichi, Japan (O.M.); Department of Microbiology, Nagoya University School of Medicine, Showa-ku, Nagoya, Japan (T.H.). Correspondence should be addressed to K-I. I. (e-mail: kenisobe@nils.go.jp).*

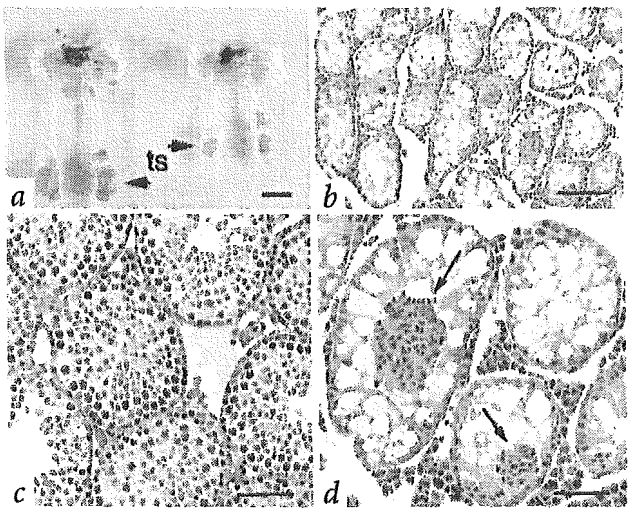

Fig. 2 Typical appearance of testes in infertile *Zfp148*$^{+/-}$ chimeric mice. *a*, Testis in 4-mo-old infertile *Zfp148*$^{+/-}$ chimeric mice or *Zfp148* wild-type chimeric mice. Testes of infertile mutant chimeric mice (right) were markedly smaller and weighed an average of 80% less (21.9 ± 1.8 mg; $n = 6$ from three chimeras) than testes of control chimeric mice (left; 113 ± 6 mg; $n = 6$ from three chimeras). No overt abnormality was detected in attached tissues. *r* = Bar, 10 mm. Arrow indicates testes (ts). *b–d*, Histological sample of testis of 4-mo-old *Zfp148* wild-type control chimeric mice (*c*) and from *Zfp148*$^{+/-}$ chimeric mice (*b,d*; *d* is higher magnification of *b*). In the mutant testis, no spermatogonia were visible, and tubules were filled by Sertoli cells (*b,d*). Hematoxylin-positive structures (arrow), which might be debris of Sertoli cells, were detected in some tubules (*d*). *r* = Bar, 150 μm (*b*) or 50 μm (*c,d*).

gonads during mouse embryogenesis (Fig. 1*a–f*). *In situ* hybridization shows that *Zfp148* mRNA is strongly expressed in male and female gonads at E12.5 but declines from E12.5 to E13.5 (data not shown). *Zfp148* is primarily expressed in primordial germ cells (PGCs), which can be recognized as large cells with large nuclei (Fig. 1*c,f*).

In this study, we investigated the role of *Zfp148* in germ cells during mouse development. We generated *Zfp148*$^{+/-}$ mouse embryonic stem (ES) cells by gene targeting and injected them into blastocysts to create chimeric *Zfp148* heterozygotes. The targeted *Zfp148* allele had a deletion of exon 9, which corresponds to >60% of the *Zfp148* coding region (Fig. 1*g,h*). Five of 1,200 doubly resistant clones had the correct targeting event, and we used 4 of these for blastocyst injection. We obtained chimeric mice from injections with *Zfp148*$^{+/-}$ ES cells but did not observe germ-line transmission of the mutated allele of *Zfp148* in these mice. Some chimeras with a high proportion of *Zfp148*$^{+/-}$ cells were infertile (five of nine *Zfp148*$^{+/-}$chimeras were infertile, and the remaining four did not show germ-line transmission; see Web Table A online). In contrast, normal germ-line transmission occurred in control chimeric mice (6 of 11 control chimeras showed germ-line transmission; see Web Table A online) using non-targeted ES cells from the same screening (defined as control ES cells). These results suggest that chimeric mice become infertile owing to heterozygosity with respect to *Zfp148* in the male germ line.

Northern-blot analysis showed that transcription of *Zfp148* was 50% lower in *Zfp148*$^{+/-}$ ES cells than in control ES cells (Fig. 1*i*). Western-blot analysis indicated that full-length 89-kDa Zfp148 was expressed in *Zfp148*$^{+/-}$ and control ES cells, and we found no evidence that truncated forms of Zfp148 were produced from the mutated allele (data not shown). These results suggest that the infertility of *Zfp148*$^{+/-}$ chimeric mice is due to the haploinsufficiency of *Zfp148* and not to the expression of a dominant negative or otherwise abnormal form of the protein.

The testes of infertile chimeric *Zfp148* heterozygotes were much smaller than those of fertile, germ-line chimeras from control ES cells (Fig. 2*a*). Histological analyses showed that gametes were completely absent and that the seminiferous tubules were populated only with Sertoli cells (Fig. 2*b–d*). This phenotype is similar to the human Sertoli cell–only syndrome[5,6].

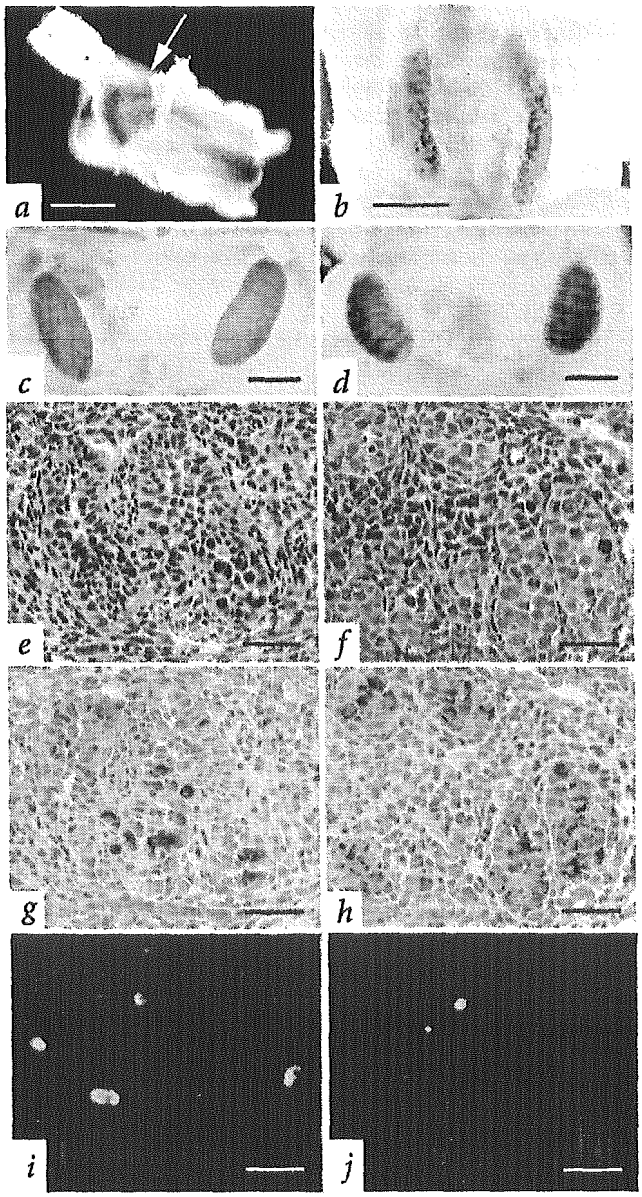

Fig. 3 Reduction in PGCs in gonads of tetraploid *Zfp148*$^{+/-}$ chimeric embryos. Whole-mount alkaline-phosphatase staining of E8.5 (*a*), E11.5 (*b*) and E13.5 *Zfp148*$^{+/-}$ tetraploid embryos (*c*) and E13.5 control tetraploid embryos (*d*). In E8.5 and E11.5 tetraploid chimeric embryos, the appearance and migration of PGCs from *Zfp148*$^{+/-}$ ES cells seemed normal (*a,b*). Gonads of E13.5 *Zfp148*$^{+/-}$ tetraploid embryos had fewer alkaline phosphatase–positive cells and weaker ladder formation (*c,d*). *e–j*, Histological analyses of tetraploid chimeric gonads. Hematoxylin and eosin staining (*e,f*), immunohistochemistry with a PGC-specific antibody 4C9 (*g,h*) and TUNEL staining (*i,j*) of E13.5 *Zfp148*$^{+/-}$ tetraploid embryos (*e,g,i*) and control tetraploid embryos (*f,h,j*). The gonads of *Zfp148*$^{+/-}$ tetraploid embryos had fewer PGCs by hematoxylin and eosin staining and by immunohistochemistry with a PGC-specific 4C9 antibody and more TUNEL-positive cells than gonads of control tetraploid embryos. *r* = Bar, 500 μm (*a,b*), 1.0 mm (*c,d*), 50 μm (*e–h*) or 150 μm (*i,j*).

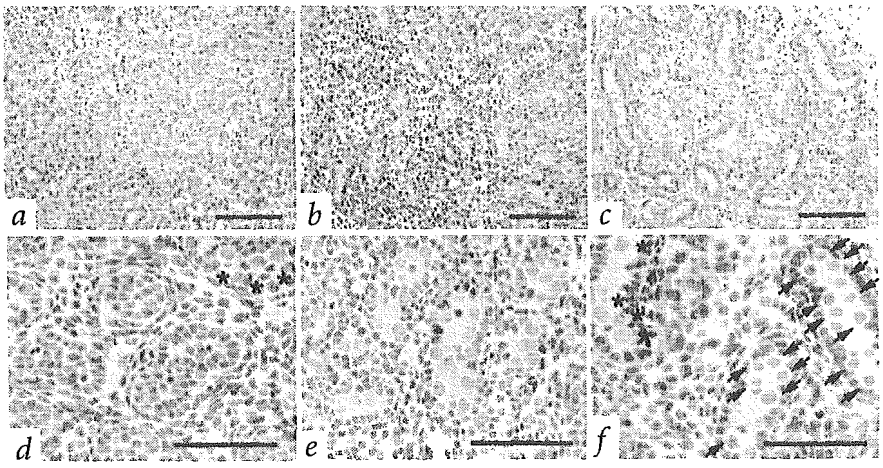

Fig. 4 Complete loss of pro-spermatogonia in E18.5 mutant chimeric embryos. Chimeric embryos were generated by injection of ES cells into ROSA26 diploid blastocysts[20]. ES cell lineage can be distinguished from host cells of ROSA26 embryos by staining the embryos with X-gal, and only blastocyst-derived cells were stained blue. After staining of whole testes with X-gal, sections were counterstained with nuclear fast red. The panels show testes derived mostly from *Zfp148*$^{+/-}$ ES cells (*a*, higher magnification in *d*), testes derived partly from *Zfp148*$^{+/-}$ ES cells (*b*, higher magnification in *e*) and testes derived mostly from control ES cells (*c*, higher magnification in *f*). When chimeric testes were derived mostly from *Zfp148*$^{+/-}$ ES cells (*a*), Sertoli cells were mostly negative for lacZ (white). In these testes, there were small numbers of lacZ-positive pro-spermatogonia (asterisk), but no lacZ-negative pro-spermatogonia from *Zfp148*$^{+/-}$ ES cells were detected (*a*,*d*), indicating that pro-spermatogonia were derived only from ROSA26 host blastocysts (asterisk) and that they could survive even they were surrounded by *Zfp148*$^{+/-}$ (white) Sertoli cells. In contrast, when chimeric testes were derived mostly from host embryos, they contained many lacZ-positive pro-spermatogonia and Sertoli cells (*b*,*e*), but no lacZ-negative pro-spermatogonia from *Zfp148*$^{+/-}$ ES cells were detected. Pro-spermatogonia derived from control ES cells developed normally in chimeric testes (arrow) with some lacZ-positive pro-spermatogonia from host embryos (asterisk; *c*,*f*). *r* = Bar, 100 μm (*a*–*c*) or 50 μm (*d*–*f*).

It is possible that testes of chimeric *Zfp148* heterozygotes lacked gametes because they never formed or because the gametes formed in early embryogenesis but were lost at a later stage. To distinguish between these possibilities, we generated tetraploid chimeric embryos from *Zfp148*$^{+/-}$ ES cells and examined the PGCs. Tetraploid blastocysts contribute little to embryonic tissues but do contribute to the extra-embryonic tissues; in contrast, ES cells contribute only to embryonic tissues[7]. By generating tetraploid chimeric embryos with *Zfp148*$^{+/-}$ ES cells, we could form *Zfp148*$^{+/-}$ PGCs and observe them in the absence of PGCs from the host blastocyst (defined as *Zfp148*$^{+/-}$ tetraploid embryos).

At E8.0–E8.5, we detected *Zfp148*$^{+/-}$ PGCs at the base of the allantois around the hindgut pocket (Fig. 3*a*). PGCs appeared normal at E11.5, increasing in number and migrating into the genital ridges (Fig. 3*b*). *Zfp148*$^{+/-}$ tetraploid embryos appeared morphologically comparable to the control tetraploid embryos at these stages. But at E13.5, alkaline-phosphatase activity was weaker in the gonads of *Zfp148*$^{+/-}$ tetraploid embryos than in those of tetraploid chimeric embryos from control ES cells (defined as control tetraploid embryos; Fig. 3*c*,*d*).

Pro-spermatogonia are large male germ cells that differentiate from PGCs and can be identified by staining with hematoxylin and eosin (Fig. 3*f*) or 4C9 antibody (refs. 8,9; Fig. 3*h*). The number of pro-spermatogonia was much lower in *Zfp148*$^{+/-}$ tetraploid embryos (Fig. 3*e*,*g*) than in control tetraploid embryos (Fig. 3*f*,*h*), which is consistent with whole-mount alkaline-phosphatase staining of gonads (Fig. 3*c*,*d*). TUNEL staining showed more large positive cells (probably pro-spermatogonia) in tubules of *Zfp148*$^{+/-}$ tetraploid embryos than in tubules of control tetraploid embryos (Fig. 3*i*,*j*). These results strongly suggest that haploinsufficiency of *Zfp148* caused apoptotic cell death of pro-spermatogonia.

We also injected *Zfp148*$^{+/-}$ ES cells into lacZ-positive ROSA26 diploid blastocysts and examined the embryos at E18.5. These chimeric embryos produced a few lacZ-positive pro-spermatogonia derived from the host blastocyst (Fig. 4) but no lacZ-negative pro-spermatogonia from *Zfp148*$^{+/-}$ ES cells (Fig. 4*a*,*d*). This indicates that *Zfp148*$^{+/-}$ pro-spermatogonia were not rescued by wild-type Sertoli cells. The *Zfp148*$^{+/-}$ pro-spermatogonia probably entered apoptosis before E18.5.

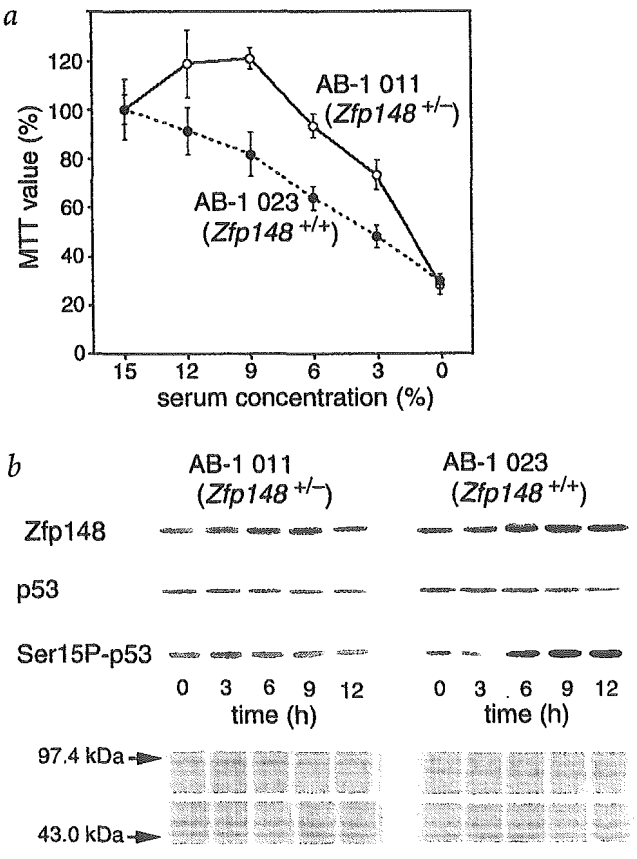

Fig. 5 Phosphorylated p53 and cell-cycle-arrest induction in control ES cells and its impairment in *Zfp148*$^{+/-}$ ES cells. *a*, MTT assay of *Zfp148*$^{+/-}$ ES cells and control ES cells after 24 h of serum starvation. Data are the mean ± s.d. of eight samples. The same experiment was done more than three times and showed the same pattern. Although the proliferation of control ES cells (clone 023, closed circle) decreased with decreasing serum concentration, *Zfp148*$^{+/-}$ ES cells (clone 011, open circle) were resistant to serum starvation. *b*, Western-blot analyses of Zfp148, p53 and Ser15P-p53 in *Zfp148*$^{+/-}$ and control ES cells after serum starvation (3% serum). Zfp148 and Ser15P-p53 were upregulated in control ES cells (clone 023, right panel), but *Zfp148*$^{+/-}$ ES cells did not upregulate Zfp148 and Ser15P-p53 to the same extent as the control (clone 011, left panel). No upregulation of p53 was observed in either control or *Zfp148*$^{+/-}$ ES cells. Coomassie brilliant blue–stained SDS–PAGE samples are shown to confirm equal sample loading.

Recent studies[1,3,4] and this study suggest that *Zfp148* may regulate cell-cycle arrest in pro-spermatogonia through p53 or $p21^{waf1}$ at E13.5. For this reason, we examined the expression and phosphorylation of p53 in serum-starved $Zfp148^{+/-}$ ES cells. Previous studies have shown that phosphorylation of p53 at Ser15 and Ser20 is essential for p53-dependent cell-cycle arrest[10,11]. Proliferation was inhibited in serum-starved control ES cells (Fig. 5*a*); in contrast, $Zfp148^{+/-}$ ES cells continued to proliferate at a higher rate than did control cells and were less sensitive to serum starvation (Fig. 5*a*). Expression of Zfp148 and phosphorylation of p53 at Ser15 (Ser15P-p53) increased in control but not $Zfp148^{+/-}$ ES cells (Fig. 5*b*). This suggests that Zfp148 regulates phosphorylation of p53 at Ser15 and that a lower level of Ser15P-p53 may contribute to loss of cell-cycle arrest in $Zfp148^{+/-}$ ES cells.

We also examined expression of Zfp148 and phosphorylation of p53 in wild-type and $Zfp148^{+/-}$ fetal germ cells *in vivo*. We isolated wild-type E12.5–E13.5 male gonads and $Zfp148^{+/-}$ E13.5 male gonads from tetraploid embryos and examined them by immunohistochemistry (Fig. 6). In wild-type male gonads, Zfp148 (Fig. 6*b*), Ser15P-p53 (Fig. 6*e*) and p53 (Fig. 6*h*) were expressed strongly at E13.5 but weakly at E12.5 (Fig. 6*a*,*d*,*g*). p53 localized primarily to the cytoplasm, but Ser15P-p53 localized to the nucleus (Fig. 6*e*,*h*). We observed similar results in female gonads from wild-type embryos (see Web Fig. A online). In $Zfp148^{+/-}$ tetraploid chimeric embryos, Zfp148 and p53 were expressed very weakly at E13.5 (Fig. 6*c*,*i*), and Ser15P-p53 was not detectable in germ cells positive for 4C9 antibody (Fig. 6*c*,*f*). These results suggest that homozygosity with respect to wild-type *Zfp148* is required for phosphorylation of p53 at Ser15 in E13.5 germ cells and that haploinsufficiency of *Zfp148* leads to loss of Ser15P-p53.

The results presented here show that $Zfp148^{+/-}$ ES cells were impaired in p53-dependent cell-cycle arrest. Despite this fact, $Zfp148^{+/-}$ germ cells did not continue to proliferate in gonads. In addition, TUNEL-positive cells were observed more frequently in $Zfp148^{+/-}$ gonads than in wild-type gonads, suggesting that deficiency in *Zfp148* led to abnormal growth or differentiation, which triggered apoptosis in fetal germ cells at approximately E13.5. The fact that *Trp53*-deficient mice do not show overt gonadal abnormalities or infertility[12] might be explained by the fact that *Trp53* is a member of a gene family that includes *Trp73* and *Trp63*. Thus, partial redundancy for function of *Trp53* might compensate for loss of *Trp53* during germ-cell development. But male *Trp53*-hypomorphic mice experience gamete degeneration after birth[13], suggesting that a reduced level of p53 cannot be complemented by other genes in the *Trp53* family.

Unlike *Trp53*, *Zfp148* is not a member of a family of related genes in the mouse, so haploinsufficiency of *Zfp148* cannot be complemented by a gene with redundant function. An alternative explanation for the difference in phenotype of *Trp53*-null and $Zfp148^{+/-}$ mice is that heterozygosity with respect to *Zfp148* might cause altered p53 function, whereas loss of *Trp53* causes complete loss of p53 function, and that these two functional states for p53 may have different phenotypic consequences during development. Previous studies also indicate that a mutation in *Atm* in humans and mice causes complete lack of male gametes[14], which may be mediated by altered Atm-dependent phosphorylation of p53 at Ser15 (ref. 15). In these mutants, however, germ-cell degeneration by apoptosis occurs during early meiosis after birth[16,17]. These results suggest that *Zfp148* and *Atm* both contribute to a complex mechanism for regulating p53, and may have different functions in the differentiation of germ cells. Further studies are needed to address how *Zfp148* regulates phosphorylation of p53 and whether impaired phosphorylation of Ser15-p53 directly leads to loss of fetal germ cells in the male gonad.

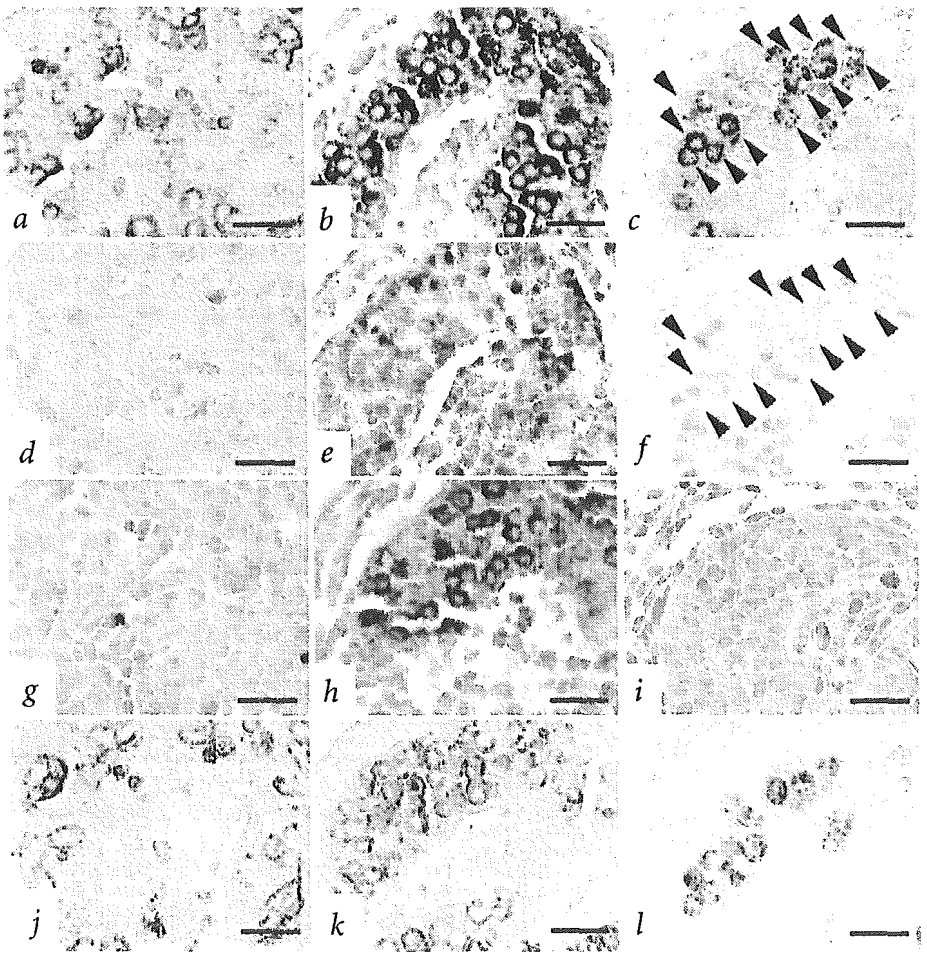

Fig. 6 Zfp148 and phosphorylated p53 induction in pro-spermatogonia at E13.5 in the male gonad. Antibodies against Zfp148 (*a–c*), Ser15P-p53 (*d–f*), p53 (*g–i*) and pre-immune rabbit serum as negative control (*j–l*) were used for E12.5 (*a*,*d*,*g*,*j*) and E13.5 (*b*,*e*,*h*,*k*) male mouse gonads of wild-type embryos and E13.5 male gonads of $Zfp148^{+/-}$ tetraploid embryos (*c*,*f*,*i*,*l*). The germ cell–specific antibody 4C9 was also used to detect germ cells (*a–c*,*j–l*). In *a–c*, Zfp148 expression was visualized with NBT/BCIP (blue), and the presence of embryonic germ cells was visualized with diaminobenzidine (brown). In *d–i*, Ser15P-p53 or p53 was visualized with NBT/BCIP (blue), and sections in *g–i* were counterstained with nuclear fast red (pink) as well. Expression of Zfp148, Ser15P-p53 and p53 were low at E12.5 but upregulated at E13.5 in the wild-type gonads. Expression of Zfp148 and p53 in the $Zfp148^{+/-}$ gonads at E13.5 were much weaker than age-matched wild-type gonads. Ser15P-p53 signal was not detected in pro-spermatogonia (indicated by arrowheads that correspond to 4C9-positive cells in *c*) in $Zfp148^{+/-}$ gonads (*f*). No signal was detected at all after NBT/BCIP staining with pre-immune, normal rabbit serum (*j–l*). *r* = Bar, 25 μm.

In summary, this study shows that haploinsufficiency of *Zfp148*, an autosomal gene, causes infertility, and that two functional copies of *Zfp148* are required for fetal germ cells to survive in male mouse gonads. A putative mechanism for this effect is suggested by the fact that Zfp148 and Ser15P-p53 are induced in wild-type but not *Zfp148*$^{+/-}$ male germ cells. Thus, *Zfp148* may have an essential role in differentiation of fetal germ cells by stimulating phosphorylation of p53 at Ser15.

Methods

Generation of *Zfp148*$^{+/-}$ ES cells and chimeric mice. We isolated *Hind*III/*Nsi*I 5′ (2.7-kb) and *Bam*HI/*Kpn*I 3′ (4.5-kb) fragments of *Zfp148* from a 129/SvJ mouse genomic library and used them to construct a replacement gene-targeting vector (Fig. 1*g*). We inserted a neomycin-resistance gene with a phosphoglycerokinase promoter (PGK-neo) between the *Nsi*I and *Bam*HI sites, deleting more than 60% of the coding region of *Zfp148*. We added a cassette expressing diphtheria toxin A to the long homology arm of the construct. We carried out ES cell targeting and chimera production as described elsewhere[18]. We identified five correctly targeted clones and used another three clones from this screen as controls, after confirming that both alleles of *Zfp148* were intact. We confirmed that both *Zfp148*$^{+/-}$ ES cell lines (clone 011, 012, 013, 014) and control ES cell lines (clone 021, 023, 025) were euploid (40 chromosomes) and carried a Y chromosome.

Production of ES cell-derived embryos. We prepared tetraploid blastocysts by fusing 2-cell stage embryos from CD-1 females, culturing them to blastocyst stage using a previously described protocol[19] and carrying out standard blastocyst injection. To generate ROSA26 blastocysts[20], homozygous ROSA26 males were mated with C57BL/6J females, and embryos were injected in the usual manner. We recovered embryos at E8.0–18.5. We carried out β-galactosidase staining as described[21]. Mice used in this study were treated according to *NIH Guide for Care and Use of Laboratory Animals*, with procedures approved by the National Institute for Longevity Sciences Animal Committees.

***In situ* hybridization.** We carried out *in situ* hybridization as previously described[22] with modifications. Briefly, we fixed embryos with 4% paraformaldehyde, dehydrated them, embedded them in paraffin and prepared sections of 7 μm. We labeled antisense and sense RNA probes corresponding to coordinates bp 1,634–2,229 of *Zfp148* with digoxigenin. We visualized the RNA probe with Fab fragments from antibody against digoxigenein conjugated with alkaline phosphatase (Roche) and 5-bromo-4-chloro-3-indolyl-phosphate (BCIP)/nitroblue tetrazolium (NBT) solutions and counterstained with methyl green. For northern-blot analysis of the targeted and non-targeted ES clones, we loaded 20 μg of total RNA per lane and quantified radioactive signals with an image analyzer system (BAS 2500, Fuji Film).

Histological analysis. We fixed embryo and adult testes with Bouin's or 4% paraformaldehyde, dehydrated them and embedded them in paraffin. We prepared sections of 5–7 μm and stained them with hematoxylin and eosin. After staining for β-galactosidase, we used nuclear fast red as a counterstain. We purchased antibody against PGC, 4C9 (LEX-2, rat IgM antibody; refs. 8,9) from Funakoshi, visualized by staining with diaminobenzidine and counterstained the sections with hematoxylin. We raised rabbit polyclonal antibody against Zfp148 against a synthetic polypeptide according to standard protocol. The antigenic Zfp148 polypeptide corresponded to amino acids 452–466 of Zfp148 (EGP SKP VHS STN YDD). We purchased rabbit polyclonal antibodies against p53, against Ser15P-p53 and against Ser20P-p53 from Cell Signaling Technology, visualized with NBT/BCIP staining and counterstained them with nuclear fast red.

Whole-mount staining of embryos for PGCs. We fixed E8.0–13.5 embryos with 4% paraformaldehyde and stained for alkaline-phosphatase activity with Fast-Red[23].

3-(4,5-dimethylthiazol-2-yl)-2,5-diphenyl tetrazolium bromide (MTT) assay and western-blot analysis. We cultured mutant *Zfp148*$^{+/-}$ and control, non-targeted ES cells on STO feeder cells in ES medium (Dulbecco's modified Eagle's medium with 15% fetal bovine serum, 2 mM glutamine and 0.1 M 2-mercaptoethanol). To prevent contamination of feeder cells, we cultured ES cells on gelatinized plates for more than two passages in ES medium. We used leukocyte inhibitory factor to prevent differentiation. We seeded 1.0×10^4 ES cells per well on 96-well plates for 16 h, and then transferred cells to ES medium with variable serum concentration. The MTT assay was done 24 h after serum starvation treatment using a Cell Counting Kit (Dojindo). For western blots, we prepared ES cells as described for the MTT assay and plated them on gelatinized plates. We prepared nuclear extracts at the indicated time after transfer to 3% serum. We used a 5-μg sample for western-blot analysis. We stained SDS–PAGE gels with Coomassie brilliant blue to confirm equal sample loading in each gel lane.

Note: Supplementary information is available on the Nature Genetics website.

Acknowledgments

We thank E.M. Eddy, G.-Q. Zhao, Y. Matsui, P. Koopman and R. Newbold for helpful discussion; R. Behringer and A. Bradley for use of AB-1 ES cells; T. Castranio for advice on production of tetraploid chimeras; M. Suzuki for technical advice on blastocyst injection; T.C., G. Scott and S. Kishigami for critical reading of the manuscript; S. Ito for helping experiment of chromosomal count of ES cells; and Y. Takeuchi, Y. and K. Mishina and Chata for encouragement. This study was supported by the Fund for Comprehensive Research on Aging and Health.

Competing interests statement

The authors declare that they have no competing financial interests.

Received 6 September; accepted 25 November 2002.

1. Bai, L. & Merchant, J.L. ZBP-89 promotes growth arrest through stabilization of p53. *Mol. Cell. Biol.* **21**, 4670–4683 (2001).
2. Hasegawa, T., Takeuchi, A., Miyaishi, O., Isobe, K. & de Crombrugghe, B. Cloning and characterization of a transcription factor that binds to the proximal promoters of the two mouse type I collagen genes. *J. Biol. Chem.* **272**, 4915–4923 (1997).
3. Hasegawa, T., Xiao, H. & Isobe, K. Cloning of a GADD34-like gene that interacts with the zinc-finger transcription factor which binds to the p21(WAF) promoter. *Biochem. Biophys. Res. Commun.* **256**, 249–254 (1999).
4. Bai, L. & Merchant, J.L. Transcription factor ZBP-89 cooperates with histone acetyltransferase p300 during butylate activation of p21(waf1) transcription in human cells. *J. Biol. Chem.* **275**, 30725–30733 (2000).
5. Rosai, J. (ed.) Male reproductive system, atrophy and infertility. in *Ackerman's Surgical Pathology* 1260–1265 (Mosby, St. Louis, 1996).
6. Wong, T.W., Straus, F.H. & Warner, N.E. Testicular biopsy in the study of male infertility. I. Testicular cause of infertility. *Arch. Pathol.* **95**, 151–159 (1973).
7. Nagy, A. *et al.* Embryonic stem cells alone are able to support fetal development in the mouse. *Development* **110**, 815–821 (1990).
8. Matsui, Y., Zsebo, K. & Hogan, B.L. Derivation of pluripotential embryonic stem cells from murine primordial germ cells in culture. *Cell* **70**, 841–847 (1992).
9. Yoshinaga, K., Muramatsu, H. & Muramatsu, T. Immunohistochemical localization of the carbohydrate antigen 4C9 in the mouse embryo: a reliable marker of mouse primordial germ cells. *Differentiation* **48**, 75–82 (1991).
10. Momand, J., Zambetti, G.P., Olson, D.C., George, D. & Levine, A.J. The *mdm-2* oncogene product forms a complex with the p53 protein and inhibits p53-mediated transactivation. *Cell* **69**, 1237–1245 (1992).
11. Thut, C.J., Goodrich, J.A. & Tjian, R. Repression of p53-mediated transcription by MDM2: a dual mechanism. *Genes Dev.* **11**, 1974–1986 (1997).
12. Donehower, L.A. *et al.* Mice deficient for p53 are developmentally normal but susceptible to spontaneous tumors. *Nature* **356**, 215–221 (1992).
13. Rotter, V. *et al.* Mice with reduced levels of p53 protein exhibit the testicular giant-cell degenerative syndrome. *Proc. Natl. Acad. Sci. USA* **90**, 9075–9079 (1993).
14. Barlow, C. *et al.* Atm-deficient mice: a paradigm of ataxia telangiectasia. *Cell* **86**, 159–171 (1996).
15. Banin, S. *et al.* Enhanced phosphorylation of p53 by ATM in response to DNA damage. *Science* **281**, 1674–1677 (1998).
16. Xu, Y. *et al.* Targeted disruption of *ATM* leads to growth retardation, chromosomal fragmentation during meiosis, immune defects, and thymic lymphoma. *Genes Dev.* **10**, 2411–2422 (1996).
17. Barlow, C. *et al. Atm* deficiency results in severe meiotic disruption as early as leptonema of prophase I. *Development* **125**, 4007–4017 (1998).
18. McMahon, A.P. & Bradley, A. The *Wnt-1* (int-1) proto-oncogene is required for development of a large region of the mouse brain. *Cell* **62**, 1073–1085 (1990).
19. Wang, Z.Q., Kiefer, F., Urbánek, P. & Wagner, E.F. Generation of completely embryonic stem cell-derived mutant mice using tetraploid blastocyst injection. *Mech. Dev.* **62**, 137–145 (1997).
20. Zambrowicz, B.P. *et al.* Disruption of overlapping transcripts in the ROSA βgeo 26 gene trap strain leads to widespread expression of β-galactosidase in mouse embryos and hematopoietic cells. *Proc. Natl. Acad. Sci. USA* **94**, 3789–3794 (1997).
21. Hogan, B., Beddington, R., Costantini, F. & Lacy, E. (eds.) Techniques for visualizing genes, gene products, and specialized cell types. in *Manipulating the Mouse Embryo* 373–375 (Cold Spring Harbor Laboratory Press, Plainview, New York, 1994).
22. Takeuchi, A. *et al.* Microglial NO induces delayed neuronal death following acute injury in the striatum. *Eur. J. Neurosci.* **10**, 1613–1620 (1998).
23. Buehr, M. & McLaren, A. Isolation and culture of primordial germ cells. *Methods Enzymol.* **225**, 58–77 (1993).
24. Wang, Y., Kobori, J.A. & Hood, L. The htβ gene encodes a novel CACCC box-binding protein that regulates T-cell receptor gene expression. *Mol. Cell. Biol.* **13**, 5691–5701 (1993).
25. Taniuchi, T., Mortensen, E.R., Ferguson, A., Greenson, J. & Merchant, J.L. Overexpression of ZBP-89, a zinc finger DNA binding protein, in gastric cancer. *Biochem. Biophys. Res. Commun.* **233**, 154–160 (1997).

ACADEMIC PRESS

Biochemical and Biophysical Research Communications 295 (2002) 187–192

BBRC

www.academicpress.com

Effects of histone acetylation on transcriptional regulation of manganese superoxide dismutase gene

Kayoko Maehara,[1] Natsuko Uekawa, and Ken-Ichi Isobe*

Department of Basic Gerontology, National Institute for Longevity Sciences, 36-3 Gengo, Morioka-cho, Obu, Aichi 474-8522, Japan

Received 6 June 2002

Abstract

To better understand the link between chromatin modification and manganese superoxide dismutase (Mn-SOD) gene expression, we have investigated the level of histone acetylation at Mn-SOD proximal promoter. TSA induced the expression of Mn-SOD mRNA and its transcriptional activity in C2C12 cells. Sp1 binding sites in the proximal promoter region of Mn-SOD were transcriptionally responsive to TSA by transfection studies. We have detected a localized acetylation of histones H3 and H4, in vivo occupation by Sp1, early growth responsive-1 (Egr-1), and histone deacetylase-1 (HDAC1) in the proximal promoter region of Mn-SOD gene using chromatin immunoprecipitation assays. Our findings indicate that Mn-SOD gene expression is repressed by Sp1–HDAC1 complex. This repression is released by a localized histone acetylation and at least in parts a displacement by Egr-1 in response to TSA.

Keywords: Manganese superoxide dismutase; Histone acetylation; Transcription; Histone deacetylase-1; Transcription; Sp1; Egr-1

The acetylation of histones is thought to be involved in the destabilization and restructuring of nucleosomes, which is probably a crucial event in the control of the accessibility of DNA templates to transcriptional factors [1–3]. A current working hypothesis is that recruitment of coactivators with HAT activity by promoter-bound transcription factors results in the acetylation of histone residues of nearby nucleosomes, which increases the accessibility of the DNA to the transcription machinery [4–6]. Replicative senescence has been studied using in vitro cultured cells (reviewed in [7–9]). This system has provided information relevant to in vivo aging processes. Senescent cells show a number of phenotypic traits. The cells become enlarged with a flattened and irregular shape, exhibit increased senescence-associated β-galactosidase activity (SA-β-gal), and up-regulate the cyclin-dependent kinase inhibitors (CKIs), such as $p21^{Cip1/Waf1}$ (p21) and $p16^{INK4a}$ (p16). A wide spectrum of signals, DNA damage, oxidative stress, histone deacetylase (HDAC) inhibitors [10,11], and expression of activated oncogenes, such as ras [12], raf [13], or mitogen-activated protein kinase kinase (MEK) [14], can cause phenotypes closely resembling senescence, referred to as premature senescence. Inhibitors of HDACs, such as sodium butyrate and trichostatin A (TSA), can induce premature senescence in human diploid fibroblasts [10] and the expression of p21 in some cultured cells [11,15]. There is a significant decrease in the level of HDAC1 during replicative senescence in human fibroblasts [16]. In addition to the evidence from in vitro cultured system, silent information regulator 2 (Sir 2), a nicotinamide adenine dinucleotide (NAD)-dependent histone deacetylase, is a limiting component that promotes longevity in yeast [17,18]. A line of evidence indicates that HDACs involve in controlling the expression of subsets of genes related to senescence.

To examine the involvement of histone acetylation in Mn-SOD gene expression, we have investigated the acetylation level of histones at Mn-SOD proximal promoter and related factors in response to TSA, an

* Corresponding author. Fax: +81-562-44-6591.
E-mail address: kenisobe@nils.go.jp (K.-I. Isobe).
[1] Present address: Cell Cycle Group, Paterson Institute for Cancer Research, Christie Hospital NHS Trust, Wilmslow Road, Manchester M20 4BX, UK. Research resident of Japan Foundation for Aging and Health.

0006-291X/02/$ - see front matter
PII: S0006-291X(02)00646-0

inhibitor of HDACs. Our findings showed that Sp1–HDAC1 complex repressed Mn-SOD gene expression in untreated condition. The epigenetic regulation of Mn-SOD by Sp1–HDAC1 complex may contribute to enhance resistance to oxidative stress in senescence. This repression was released in TSA-treated cells by two distinct mechanisms, a rapid acetylation of histones H3 and H4 and a displacement of Sp1–HDAC1 complex by early growth responsive-1 (Egr-1) induced by TSA.

Materials and methods

Materials. C2C12 cells were obtained from RIKEN CELL BANK. Cell culture reagents were obtained from Gibco-BRL Life Technologies. Fetal bovine serum and TSA were obtained from Sigma. Antibodies were from the following sources: anti-acetylated histone H3, anti-acetylated histone H4, anti-Sp1, and anti-HDAC1 from Upstate Biotechnology; anti-Egr-1 and control rabbit immunoglobulin G (IgG) from Santa Cruz Biotechnology; horseradish peroxidase (HRP)-conjugated anti-rabbit-IgG from New England Biolabs. An Sp1 consensus oligonucleotide was obtained from Santa Cruz Biotechnology.

RNA isolation and analysis. The cells were preincubated in fresh serum-free medium for 24 h before the treatments. Total cytoplasmic RNA was isolated using the guanidine isothiocyanate method from the cells that were left untreated or treated with 100 ng/ml TSA for 2, 4, 8, 16, or 24 h. Samples of 10 μg total RNA were denatured, separated by electrophoresis in a 1% agarose gel containing formaldehyde, and transferred to GeneScreen membranes (DuPont, NEN). The membranes were prehybridized and then hybridized with a Mn-SOD cDNA [19], Sp1 cDNA [20], or Egr-1 cDNA probe [21] labeled with [α-^{32}P] dCTP (NEN) using a random primer labeling system (Pharmacia Biotech). After hybridization, the membranes were washed and exposed to X-ray film (Fuji Film). All blots were rehybridized with a glyceraldehyde-3-phosphate dehydrogenase (GAPDH) cDNA probe to normalize for mRNA loading differences. To quantify the contents of mRNA in the cells, the membranes were exposed to imaging plates (Fuji Film) and radioactivities were measured with a bioimage analyzer, Fijix BAS 1500 (Fuji Film).

Cell culture. C2C12 cells were maintained in Dulbecco's modified Eagle's medium, supplemented with 10% fetal bovine serum, 100 U/ml penicillin, and 100 μg/ml streptomycin.

Plasmid constructs. The mouse Mn-SOD promoter luciferase reporter plasmids were constructed as described previously [21]. The construction of reporter plasmids containing mutated sequences in Sp1 binding sites was described previously [22].

Transfection assays. Transient transfection of C2C12 cells was carried out using SuperFect Reagent (Qiagen) as previously described [22]. In general, the day before transfection, 2×10^5 cells were plated in 12-well tissue culture plates. A total of 2.5 μg DNA consisting of 2.25 μg indicated luciferase plasmid and 0.25 μg pRL-thymidine kinase control vector (pRL-TK) (Promega) per plate was used for transfection studies. After transfection, the cells were placed in serum-free medium for 24 h; 100 ng/ml TSA or control buffer was then added for an additional 16 h. After being harvested, the cells were assayed by the Dual-Luciferase Reporter Assay System (Promega), using a luminometer (EG & G Berthold). Protein concentrations of the cell lysates were determined by the method of Bradford with the Bio-Rad Protein Assay Dye Reagent. Promoter activities were expressed as relative light units (RLU), normalized against the concentration of the protein. For transfection assay using reporter plasmids containing mutated sequences in Sp1 binding sites, the luciferase activity of Mnpro (−250) in untreated cells was normalized to 100 and the relative activities were shown. All transfection experiments were repeated three times.

Western blot analysis. Nuclear extracts (20 μg) were run under reducing conditions in 8% sodium dodecyl sulfate–polyacrylamide gel electrophoresis (SDS–PAGE), transferred onto polyvinylidene difluoride membranes (Millipore, Bedford, MA), and reacted with antibodies specific for Sp1 and Egr-1. The primary antibodies were detected by counterstaining with a HRP-linked antibody and visualized by enhanced chemiluminescence.

Chromatin template immunoprecipitation (Chip). Soluble chromatin was prepared according to manufacturer's recommendations with slight modification. The equivalent of 1×10^6 cells was used per chromatin immunoprecipitation reaction. Approximately 6×10^6 C2C12 cells were grown and preincubated in fresh serum-free medium for 24 h before the treatments. Cells treated with or without 100 ng/ml TSA for indicated time were fixed by adding formaldehyde to 1% final concentration. Cross-linking was allowed to proceed at room temperature for 6 min and terminated with glycine (final concentration 125 mM). Cells were washed with PBS, collected in lysis buffer, and sonicated on ice. A mean DNA size generated by sonication was 0.3–1.0 kb. Chromatin was precleared with salmon-sperm DNA/protein An agarose slurry for 1 h at 4 °C with rotation. Precleared chromatin was incubated with 2.5 μg of each antibody specific for acetylated histones H3 and H4, Sp1, and HDAC1 or 4 μg anti-Egr-1 antibody at 4 °C with rotation. Immunocomplexes were recovered by adding 30 μl salmon-sperm DNA/protein A–agarose slurry for 1 h at 4 °C with rotation. Precipitates were successively washed with following buffers: low salt immunocomplex wash buffer (0.1% sodium dodecyl sulfate (SDS), 1% Triton X-100, 2 mM EDTA, 20 mM Tris–HCl (pH 8.1), and 150 mM NaCl), high salt immunocomplex wash buffer (0.1% SDS, 1% Triton X-100, 2 mM EDTA, 20 mM Tris–HCl (pH 8.1), and 500 mM NaCl), LiCl immunocomplex wash buffer (0.25 M LiCl, 1% Nonidet P-40, 1% deoxycholate, 1 mM EDTA, and 10 mM Tris–HCl (pH 8.1)), and 1 × TE buffer (10 mM Tris–HCl, 1 mM EDTA, pH 8.0) twice. Pellets were eluted two times in 250 μl elution buffer (1% SDS, 0.1 M $NaHCO_3$). Cross-links were reversed by incubating samples at 65 °C overnight. Samples were incubated with 20 μg proteinase K at 45 °C for 1 h, extracted with phenol:chloroform, and ethanol precipitated. Pellets were resuspended in 50 μl H_2O and utilized for quantitative polymerase chain reaction (PCR) analysis. PCR were performed in 25 μl volume with immunoprecipitated material, 10 pmol primer set, 0.5 U KOD plus DNA polymerase (Toyobo), and 1 μCi [α-^{32}P]dCTP. After 2 min of denaturation at 94 °C, samples were subjected to 30 cycles of a program consisting of 15 s at 94 °C and 1 min at 68 °C, ending with a final 7 min incubation at 72 °C. The linear range for the primer pair was determined using different amounts of input samples. The primers used to amplify Mn-SOD promoter region were 5′-GCTCGCTGG TCCGGGATGGCAGCGGCC-3′ (positions −263 to −237) and 5′-CTTTTATTCCCTTTAGCAAATTTCAA-3′ (positions −107 to −89). PCR products were electrophoresed on 8% polyacrylamide gels and quantified on a Fuji phosphorimager.

Results and discussion

TSA enhances the expression of Mn-SOD

C2C12 cells were treated with TSA to examine the effect on Mn-SOD gene expression. Mn-SOD mRNA was increased in the first 2 h with TSA treatment. The level of Mn-SOD mRNA in TSA-treated cells peaked at 8 h with a threefold induction compared to the level in the untreated cells (data not shown).

Mn-SOD promoter contains regulatory DNA elements responsive to TSA

A series of Mn-SOD promoter plasmids was transiently transfected into C2C12 cells and then treated with 100 ng/ml TSA for 16 h. The promoter activity was normalized against the concentration of the protein, because the activity of pRL-TK control vector was induced by TSA. Constructs containing 231, 250, 538, and 1452 bp of 5′ flanking DNA exhibited a high

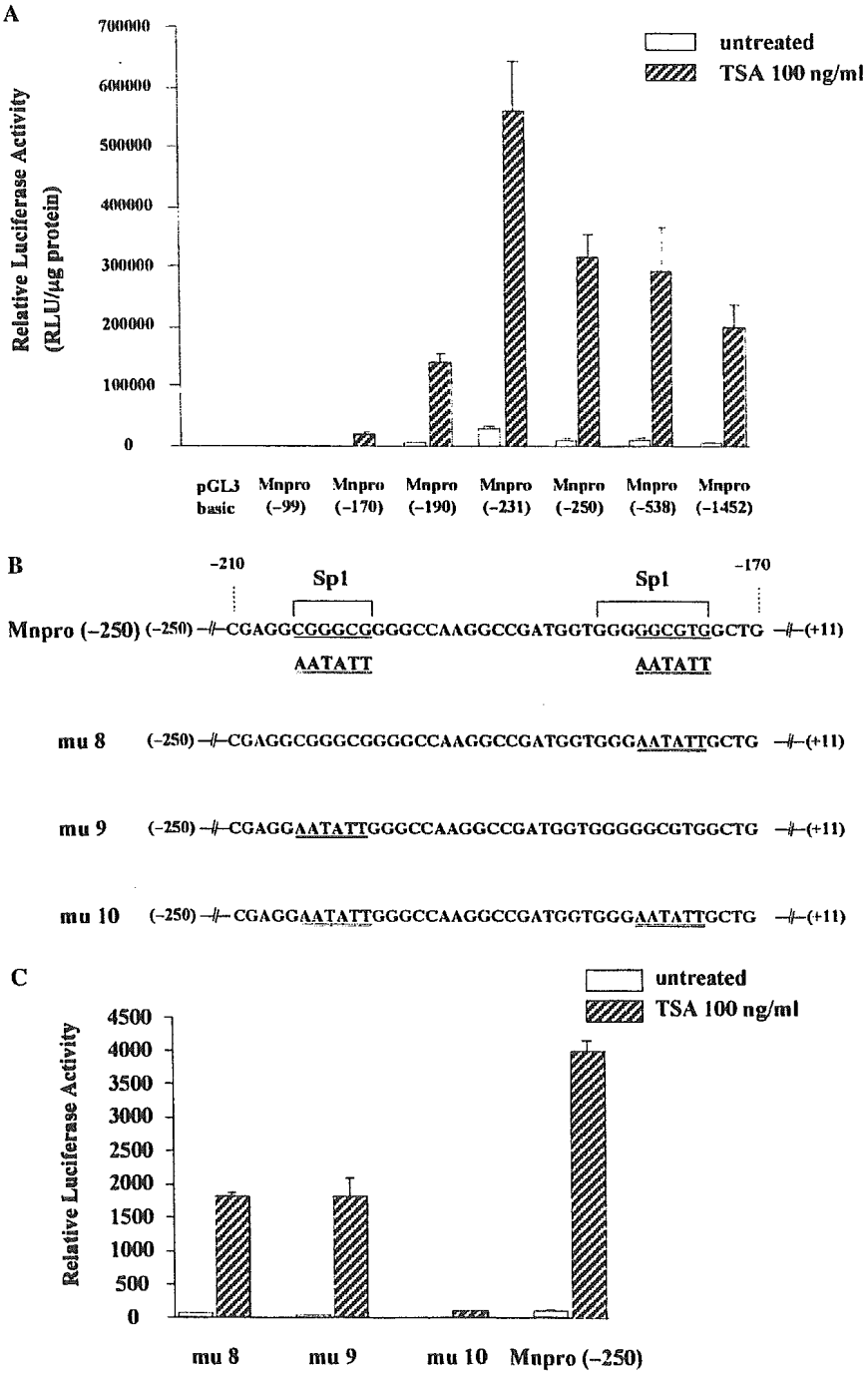

Fig. 1. Functional analysis of the Mn-SOD promoter. (A) C2C12 cells were transfected with luciferase reporter constructs containing the 5′ flanking DNA of the Mn-SOD gene and then treated with 100 ng/ml TSA for 16 h. Promoter activities are expressed as relative light units (RLU), normalized against the concentration of the protein. The positions of the bases are indicated relative to the Mn-SOD transcription initiation site (+1). (B) Reporter plasmids containing mutated sequences (mu 8, mu 9, and mu 10) in Sp1 binding sites were used for transfection studies. Brackets indicated the location of the sites for Sp1. (C) C2C12 cells were transfected with luciferase reporter constructs containing mutated sequences and then treated with 100 ng/ml TSA for 16 h. The luciferase activity of Mnpro (−250) in untreated cells was normalized to 100 and the relative activities were shown. Results are expressed as means ± SE of three independent experiments, each performed in triplicate.

level of relative luciferase activity in the untreated cells and the activity was increased drastically by the treatment with TSA (Fig. 1A). A 231-bp fragment of Mn-SOD proximal promoter contained two GC clusters. To clarify the *cis*-elements for TSA-mediated Mn-SOD transcription, we performed luciferase assays with reporter plasmids containing the site-specific mutations introduced into the Mnpro (−250) (Fig. 1B). The mutations of the Sp1 binding sites (Sp1 and Egr-1 binding sites) reduced the transcriptional activity in untreated cells (Fig. 1C). Abrogation of one of the Sp1 sites (mu 8 and mu 9) caused a 50% reduction of TSA-induced transcriptional activity compared with that of the cells transfected with Mnpro (−250). Mutations of both sites for Sp1 (mu 10) led to a marked loss of TSA-induced transcriptional activity. Transfection studies indicated that Sp1 protein was a crucial factor for TSA-mediated Mn-SOD transcription. EMSA experiments showed that the binding elements of Egr-1 and Sp1 family proteins overlapped and Egr-1 competed with Sp1 for binding to Mn-SOD promoter (data not shown).

Acetylation level of histones H3 and H4 correlates with Mn-SOD transcriptional activation

We investigated the possibility that TSA stimulation results in the acetylation of histones H3 and H4 within Mn-SOD promoter. We immunoprecipitated formamide cross-linked, sonicated chromatin fragments from the untreated cells and TSA-treated cells using antibodies specific for the acetylated histones H3 and H4 (Figs. 2A and B). Input corresponded to PCR containing 0.5% total amount of chromatin used in immunoprecipitation reactions. An enhancement of acetylated histones H3 and H4 was rapidly observed in Mn-SOD proximal promoter after TSA stimulation in C2C12 cells. Increased acetylation level of histones H3 and H4 sustained over twofold in 6 h after stimulation compared with the level of untreated cells. The levels of localized acetylation of histones H3 and H4 declined gradually and reduced to the level of the untreated cells in 15 h and 24 h after stimulation, respectively. A localized acetylation of histones H3 and H4 at Mn-SOD promoter occurred concomitantly with its gene expression in TSA-treated cells (Fig. 2B).

In vivo occupancy by Sp1, Egr-1 and HDAC1

Mn-SOD promoter has GC clusters bound by Sp1 family proteins and Egr-1 (data not shown). We performed Chip assays to analyze in vivo occupancy of the related factors to Mn-SOD promoter (Fig. 2). Sp1 binding to the proximal promoter was detected in the untreated cells. The binding by Sp1 was increased in 1 h and then reduced by 9 h, following TSA treatment. After

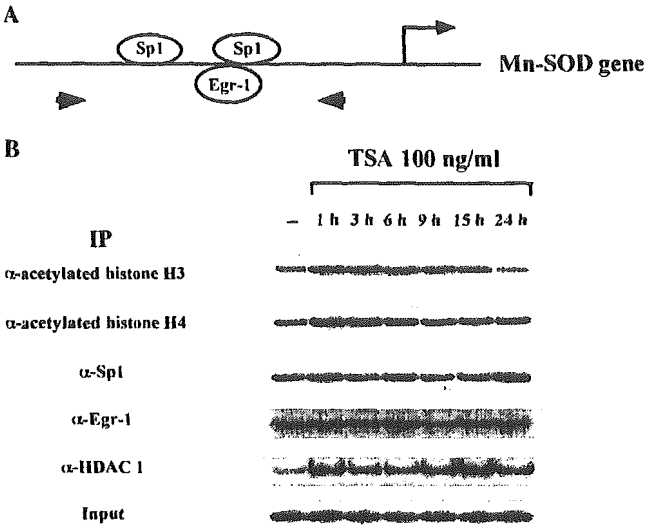

Fig. 2. A localized histone acetylation and in vivo occupancy by Sp1, Egr-1, and HDAC1 in Mn-SOD promoter. (A) Mn-SOD proximal promoter was examined in Chip assay. Sp1 and Egr-1 binding sites are shown. Small arrows indicated a primer pair of Mn-SOD gene, positions −263 to −237 and −107 to −89. Large arrow indicated a transcription start site. (B) Antibodies specific for acetylated histones H3 and H4, Sp1, Egr-1, and HDAC1 were used to immunoprecipitate chromatin. PCR was performed with the primer pair of Mn-SOD gene. Amplified products were detected by autoradiography. Input corresponded to PCR containing 0.5% total amount of chromatin used in immunoprecipitation reactions.

that, Sp1 occupancy was gradually increased again in TSA-treated cells. In contrast to Sp1 binding, the intensity of Egr-1 binding to Mn-SOD promoter gradually increased from 1 h to 3 h and peaked at 6 h in TSA-treated cells. This result was consistent with the results that Egr-1 was synthesized in response to TSA shown in Figs. 3A and B. In vivo occupancy by HDAC1 to the promoter was slightly detected in the untreated cells and strongly detected in the cells within 1 h after TSA stimulation. HDAC1 occupancy was drastically reduced in the treated cells for 6 h and then increased by 15 h after TSA treatment. This pattern was reminiscent of that of Sp1 binding observed in the cells, indicating the possibility that HDAC1 was recruited by the association with Sp1.

Egr-1 expression is induced by TSA

We analyzed the expression of Sp1 and Egr-1 in response to TSA. Nuclear extracts were subjected to SDS–PAGE and Western blot analysis. As shown in Fig. 3A, Sp1 family proteins were expressed constitutively in nuclear extracts prepared from both untreated and TSA-treated cells. In contrast, Egr-1 was induced in the nuclear extracts prepared from TSA-treated cells. The expression of Sp1 mRNA was not altered by TSA treatment (Fig. 3B). After TSA stimulation, the induc-

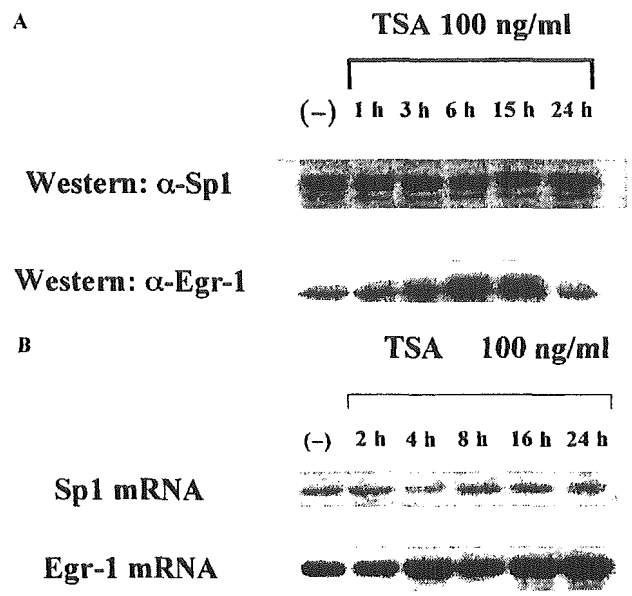

Fig. 3. TSA induces Egr-1 in C2C12 cells. C2C12 cells were left untreated or treated with 100 ng/ml TSA for the indicated time. (A) Nuclear extracts were subjected to Western blot analysis using anti-Egr-1 or Sp1 antibody. (B) Northern blot analysis using an Egr-1 or Sp1 cDNA probe.

tion of Egr-1 mRNA was detected within 4 h and maintained by 24 h.

Transcriptional activation of Mn-SOD induced by TSA was mediated by two distinct mechanisms. One is an inhibitory effect of TSA on HDAC1 activity essential for regulation of transcription. Inhibition of HDAC1 activity resulted in a rapid acetylation of histones H3 and H4 around the proximal promoter region of Mn-SOD transcriptionally responsible for TSA. We could not exclude the contribution of the other HDACs to Mn-SOD transcription. Another is a displacement of Sp1–HDAC1 complex by Egr-1 in response to TSA. Egr-1 was found to compete with Sp1 in the binding to Mn-SOD promoter shown in EMSAs and Chip assay. We previously showed that platelet-derived growth factor (PDGF) induced Mn-SOD gene expression and the mechanism of Mn-SOD transcription mediated by PDGF involved MEK1-extracellular signal-regulated kinase 1 and 2 (ERK1/2) signaling pathway and its downstream transcription factor, Egr-1 [21]. The induction of Egr-1 occurred more rapidly in PDGF-treated cells than in TSA-treated cells. This competition may play a role in regulation of promoter activity of Mn-SOD.

Acknowledgments

We thank Drs. Ye-Shih Ho (Wayne State University) for providing a rat Mn-SOD cDNA probe and Thomas Shenk (Princeton University) for providing pCGN-Sp1. We greatly thank Dr. Yasuhiko Takahashiwho who enabled us to establish the chromatin immunoprecipitation assay in our own laboratory. We are indebted to Drs. Hideo Nakajima and Mitsuo Maruyama for many helpful comments and suggestions. This study was supported by Fund for Comprehensive Research on Aging and Health, in part by the Program for Promotion of Fundamental Studies in Health Sciences of the Organization for Pharmaceutical Safety and Research (of Japan) and in part by grant-in-aids for Scientific Research from the Ministry of Education.

References

[1] M. Grunstein, Histone acetylation in chromatin structure and transcription, Nature 389 (1997) 349.
[2] C.A. Mizzen, C.D. Allis, Linking histone acetylation to transcription regulation, Cell. Mol. Life Sci. 54 (1998) 6–20.
[3] K. Struhl, Histone acetylation and transcriptional regulatory mechanism, Genes Dev. 12 (1998) 599.
[4] R.D. Kornberg, Y. Lorch, Twenty-five years of the nucleosome, fundamental particle of the eukaryote chromosome, Cell 98 (1999) 285–294.
[5] A. Imhof, X.J. Yang, V.V. Ogrizco, Y. Nakatani, A.P. Wolff, H. Ge, Acetylation of general transcription factors by histone acetyltransferase, Curr. Biol. 7 (1997) 689–692.
[6] H. Ugai, K. Uchida, H. Kawasaki, K.K. Yokoyama, The coactivator p300 and CBP have different functions during the differentiation of F9 cells, J. Mol. Med. 77 (1999) 481–494.
[7] J.R. Smith, O.M. Pereira-Smith, Replicative senescence: implications for in vivo aging and tumor suppression, Science 273 (1996) 59–63.
[8] A.S. Lundberg, W.C. Hahn, P. Gupta, R.A. Weiberg, Genes involved in senescence and immortalization, Curr. Opin. Cell Biol. 12 (2000) 705–709.
[9] M. Serrano, M.A. Blasco, Putting the stress on senescence, Curr. Opin. Cell Biol. 13 (2001) 748–753.
[10] V.V. Ogryzko, T.H. Hirai, V.R. Russanova, D.A. Barbie, B.H. Howard, Human fibroblast commitment to a senescence-like state in response to histone deacetylase inhibitors is cell cycle dependent, Mol. Cell. Biol. 16 (1996) 5210–5218.
[11] X. Hengyi, T. Hasegawa, O. Miyaishi, K. Ohkusu, K. Isobe, Sodium butyrate induces NIH3T3 cells to senescence-like state and enhances promoter activity of $p21^{WAF/CIP1}$ in p53-independent manner, Biochem. Biophys. Res. Commun. 237 (1997) 457–460.
[12] M. Serrano, A.W. Lin, M.E. McCurrach, D. Beach, S.W. Lowe, Oncogenic ras provokes premature cell senescence associated with accumulation of p53 and $p16^{INK4a}$, Cell 88 (1997) 593–602.
[13] J. Zhu, D. Woods, M. McMahon, J.M. Bishop, Senescence of human fibroblasts induced by oncogenic Raf, Genes Dev. 12 (1998) 2997–3007.
[14] A.W. Lin, M. Barradas, J.C. Stone, L. van Aelst, M. Serrano, S.W. Lowe, Premature senescence involving p53 and p16 is activated in response to constitutive MEK/MAPK mitogenic signaling, Genes Dev. 12 (1998) 3008–3019.
[15] V.M. Richon, T.W. Sandhoff, R.A. Rifkind, P.A. Marks, Histone deacetylase inhibitor selectively induces $p21^{WAF1}$ expression and gene-associated histone acetylation, Proc. Natl. Acad. Sci. USA 97 (2000) 10014–10019.
[16] M. Wagner, G. Brosch, W. Zwerschke, E. Seto, P. Loidl, P. Jansen-Dürr, Histone deacetylases in replicative senescence: evidence for a senescence-specific form of HDAC-2, FEBS Lett. 499 (2001) 101–106.
[17] M. Kaeberlein, M. McVey, L. Guarente, The SIR2/3/4/ complex and SIR2 alone promote longevity in *Saccharomyces cerevisiae* by two different mechanisms, Genes Dev. 13 (1999) 2570–2580.
[18] S. Imai, C.M. Armstrong, M. Kaeberlein, L. Guarente, Transcriptional silencing and longevity protein Sir2 is an

NAD-dependent histone deacetylase, Nature 403 (2000) 795–800.
[19] Y.-S. Ho, J.D. Crapo, Nucleotide sequences of cDNAs coding for rat manganese-containing superoxide dismutase, Nucleic Acids Res. 15 (1987) 10070.
[20] C.L. Parks, T. Shenk, The serotonin 1a receptor gene contains a TATA-less promoter that responds to MAZ and Sp1, J. Biol. Chem. 271 (1996) 4417–4430.
[21] K. Maehara, T. Hasegawa, K. Isobe, A NF-κB p65 subunit is indispensable for activating manganese superoxide dismutase gene transcription mediated by tumor necrosis factor-α, J. Cell. Biochem. 77 (2000) 474–486.
[22] K. Maehara, K. Oh-Hashi, K. Isobe, Early growth-responsive-1-dependent manganese superoxide dismutase gene transcription mediated by platelet-derived growth factor, FASEB J. (2001), 10.1096/fj.00-0909fje.

Aging and obesity augment the stress-induced expression of tissue factor gene in the mouse

Koji Yamamoto, Takayoshi Shimokawa, Hong Yi, Ken-ichi Isobe, Tetsuhito Kojima, David J. Loskutoff, and Hidehiko Saito

Hypercoagulability and thrombotic tendency are frequently induced by a variety of stressors. Clinically, aged subjects and obese patients are more susceptible to thrombotic diseases associated with stress, but the underlying mechanisms are unknown. We investigated the expression of a procoagulant gene, tissue factor (TF), in a mouse model of restraint stress. Twenty hours of restraint stress to mice caused a substantial induction of TF mRNA in several tissues. Importantly, the magnitude of induction of TF mRNA by restraint stress was larger in aged mice compared with young mice. In situ hybridization analysis of the stressed aged mice revealed that strong signals for TF mRNA were localized to renal epithelial cells, smooth muscle cells, adventitial cells, and adipocytes but not to vascular endothelial cells. These observations suggest that restraint stress induces the TF expression in a tissue-specific and cell type–specific manner. Genetically obese mice were also hyperresponsive to restraint stress in the induction of TF gene, especially in their livers and adipose tissues. Stress-induced microthrombi formation was pronounced in renal glomeruli and within the vasculature in adipose tissues of aged mice. Tumor necrosis factor-α (TNF-α) antigen in plasma was elevated by stress in aged mice and obese mice, and pretreatment of mice with anti–TNF-α antibody partially attenuated the stress-mediated induction of TF gene in adipose tissues in these mice. These results suggest that the induction of TF gene may increase the risk of stress-associated thrombosis in older and obese subjects and that TNF-α may be involved. (Blood. 2002;100:4011-4018)

Introduction

The stress response is thought to be required for the maintenance of homeostasis and is characterized by rapid changes in the gene expression of stress proteins.[1] This response is best demonstrated in the neuro-endocrine system (eg, the hypothalamic-pituitary-adrenal axis)[2] and, in this setting, may be mediated by the activation of the glucocorticoid cascade[3] and of the sympathetic nervous system.[4,5] The restraint stress model often has been used to investigate the stress response experimentally in terms of pharmacologic, physiologic, or pathologic phenomena in vivo.[6] For example, restraint stress induces the expression of heat shock protein, a typical stress protein, in the rat,[2,4] and this induction may be mediated by the sympathetic nervous system.[4,5] The induction of stress proteins may contribute to the development of a number of clinically relevant phenomena, including tissue and organ damage, and the immune response.[7] Hypercoagulability in the blood and thrombotic tendency also may be induced by physical[8,9] and mental stress.[10] In this context, aged animals[2-5] and/or obese mice[11,12] may have lower tolerance to stress insults. Clinically, older and obese individuals are susceptible to the stress-mediated pathologic changes, including thrombotic complications,[13,14] possibly because of the stress-induced imbalance in the coagulation and fibrinolytic system.

Tissue factor (TF) is the primary cellular initiator of the coagulation protease cascade and serves as a specific cofactor for plasma factors VII/VIIa.[15] TF is constitutively expressed by several extravascular cell types (eg, epithelial cells, adventitial cells, adipocytes) and is inducibly expressed by monocytes and endothelial cells within the vasculature. *Cis*-acting regulatory elements within the human TF promoter would control constitutive and inducible expression in various cell types.[16] TF gene expression appears to be regulated by a variety of transcription factors (eg, nuclear factor-κB [NF-κB], AP-1, and Egr-1)[16,17] and is activated by external signals, such as inflammatory cytokines (eg, tumor necrosis factor-α [TNF-α], interleukins), growth factors, or bacterial lipopolysaccharide. Aberrant expression of TF may be responsible for thrombotic episodes in patients with a variety of clinical disorders, including atherosclerosis,[18] sepsis,[19] and cancer.[20] A couple of studies have shown an increase in TF-mediated coagulation and/or factor VII activity in obese patients.[21] Aging is also associated with increased plasma level of factor VII, which is an independent risk factor for thrombotic disease.[22] Thus, TF/factor VII may contribute to the hypercoagulable state under a variety of pathologic conditions.

We previously reported that plasminogen activator inhibitor-1 (PAI-1) and/or antithrombin was involved in the development of renal glomerular thrombosis induced by restraint stress.[23,24] In the present study, we analyzed the gene expression of another key molecule for thrombosis, TF, in a murine model of restraint stress

From the First Department of Internal Medicine, Nagoya University School of Medicine, Aichi Blood Disease Research Foundation, Department of Medical Technology, Nagoya University School of Health Sciences, and Nagoya National Hospital, Nagoya, Japan; Department of Basic Gerontology, National Institute for Longevity Sciences, Obu, Japan; and Department of Vascular Biology (VB-3), The Scripps Research Institute, La Jolla, CA.

Submitted April 4, 2002; accepted July 11, 2002. Prepublished online as *Blood* First Edition Paper, July 25, 2002; DOI 10.1182/blood-2002-03-0945.

Supported by grants-in-aid from the Ministry of Education, Science, Sports and Culture from the Ministry of Health and Welfare, by Funds for Comprehensive Research on Aging and Health, Japan, and by grant HL-47819 (D.J.L.) from the National Institutes of Health.

Reprints: Koji Yamamoto, First Department of Internal Medicine, Nagoya University School of Medicine, 65 Tsurumai, Showa, Nagoya 466-8550, Japan; e-mail: kojiy@med.nagoya-u.ac.jp.

The publication costs of this article were defrayed in part by page charge payment. Therefore, and solely to indicate this fact, this article is hereby marked "advertisement" in accordance with 18 U.S.C. section 1734.

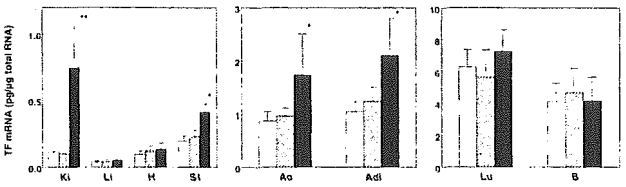

Figure 1. Changes in the expression level of TF mRNA in mouse tissues by restraint stress. Eight-week-old C57BL/6J mice were placed into restraint tubes for 2 or 20 hours, and then the tissues were removed. Total tissue RNA was prepared and analyzed for TF mRNA expression level by quantitative RT-PCR assay as described in "Materials and methods." For each tissue type, □ indicates level before stress; ▨, after 2 hours of restraint stress; and ■, after 20 hours of restraint stress. The data are represented as the means and SD (n = 8) in each amount of time under stress, and the error bars represent interanimal variation. $^{*}P < .05$; $^{**}P < .02$. Ki indicates kidney; Li, liver; H, heart; SI, small intestine; Ao, aorta; Adi, adipose (epididymal fat); Lu, lung; B, brain.

in vivo. Furthermore, we investigated the effects of aging and obesity on the stress-induced TF expression and tissue thrombosis by using extremely aged (12- and 24-month-old) mice and genetically obese (C57BL/6J ob/ob) mice. Overnight restraint stress to mice substantially induced TF mRNA expression in some tissues. More importantly, the stress-induced TF expression and/or microvascular thrombosis were pronounced in aged mice and in obese mice. Finally, endogenous TNF-α, which was also increased by stress, may be a primary mediator for the induction of TF gene in this restraint model. Thus, elevated TF expression by stress may, in part, contribute to the stress-associated thrombosis, and this response of TF gene is exacerbated by aging and obesity.

Materials and methods

Restraint stress

Male C57BL/6J mice aged 2, 12, and 24 months, were obtained from SLC Japan (Shizuoka, Japan) and through the National Institute of Aging. Mice were placed into 50-mL conical centrifuge tubes fitted with multiple punctures so as to allow ventilation. The tubes were placed in horizontal holders, and the animals thus were maintained for a continuous period of restraint.[5] During this time, the animals were provided with water only. After 2 or 20 hours of restraint, the mice were killed by overdose inhalation anesthesia with methoxyflurane (Pitman-Moore, Mundelein, MD). Tissues were rapidly removed by standard dissection techniques and were either minced and immediately frozen in liquid nitrogen for preparation of total RNA or fixed in chilled 4% paraformaldehyde and embedded in paraffin for in situ hybridization and for staining with periodic acid Schiff (PAS) or hematoxylin/eosin. This experimental protocol was approved by the animal resource committee of our university.

In separate experiments, 8-week- and 24-month-old male C57BL/6J mice were pretreated intraperitoneally either with control (nonimmune) hamster immunoglobulin G (IgG; 25 μg/mouse; Genzyme, Cambridge, MA) or with the IgG fraction of a neutralizing hamster monoclonal antibody (mAb) to mouse TNF-α (25 μg/mouse; Genzyme)[25] before 20 hours of continuous restraint stress. The blood was collected into 20 mM EDTA (ethylenediaminetetraacetic acid) (final concentration) and centrifuged at 3000*g* for 5 minutes, and then the plasma was removed and stored at −70°C. The tissues were collected and prepared as described above. Meanwhile, 6-week-old male obese mice (C57BL/6J ob/ob) and their lean counterparts (C57BL/6J +/?), both of which were obtained from The Jackson Laboratories (Bar Harbor, ME), were put into restraint tubes for 20 hours and then killed. The tissues were removed and prepared for subsequent analysis as described earlier. They were also pretreated intraperitoneally either with control hamster IgG (1 μg/g) or with hamster antimouse TNF-α antibody (1 μg/g) before 20 hours of continuous restraint stress, and the tissues were collected.

RNA extraction and quantitative RT-PCR assay

Total RNA was prepared from unfixed tissues by using the ULTRASPEC RNA ISOLATION SYSTEM (Biotecx Laboratories, Houston, TX) and then quantitated by measuring absorption at 260 nm. The content of TF mRNA in murine tissues was determined by quantitative reverse transcription–polymerase chain reaction (RT-PCR) assay by using a competitor RNA (cRNA) containing sequences of upstream and downstream primers for mouse TF and β-actin, as described previously.[26] After reverse transcription using the cRNA, ranging from 0.1 to 10 pg, and PCR amplification of 30 cycles (95°C for 1 minute, 60°C for 1 minute, and 72°C for 1 minute) using ^{32}P-end-labeled sense primer (5×10^5 cpm), 20-μL aliquots of the PCR products were electrophoresed on a 2.5% agarose gel. The appropriate bands corresponding to the cRNA product and the target mRNA product were excised from the gel, and the incorporated radioactivity in each was determined with the use of a scintillation counter. Finally, the content of TF mRNA in each tissue was determined by extrapolation using the cRNA standard curve, and the data were represented as picogram TF mRNA per microgram total RNA. All of the RT-PCR experiments were performed in triplicate. Variations in sample loading were assessed by comparison with β-actin mRNA.

Statistical analysis

Statistical analysis of all quantitative RT-PCR results was performed by using the unpaired Student *t* test. Differences were not considered significant when $P > .05$ (group size, n = 6 or 8).

Determination of TNF-α antigen in mouse plasma

Total TNF-α antigen in plasma (picogram per milliliter was measured using the ELISA-view kit (BioSource International, Camarillo, CA).

In situ hybridization

In situ hybridization was performed using ^{35}S-labeled antisense riboprobes, as described previously.[26] After hybridization, the slides were dehydrated by immersion in a graded alcohol series containing 0.3 M NH_4Ac and dried. Then the slides were coated with NTB2 emulsion (Kodak, Rochester, NY; 1:2 in water), and exposed in the dark at 4°C for 8 to 12 weeks. The slides were developed for 2 minutes in D19 developer (Kodak), fixed, washed in

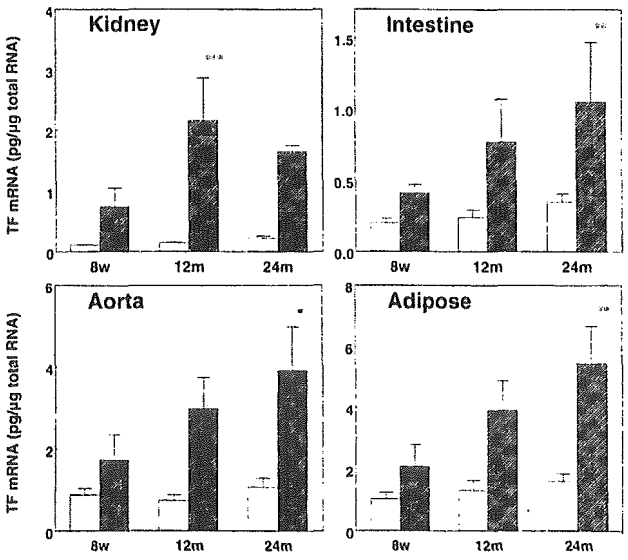

Figure 2. Induction of TF mRNA by restraint stress in the tissues of young and aged mice. The indicated tissues were removed from 8-week- (8w), 12-month- (12m), and 24-month-old (24m) C57BL/6J mice before (open bars) and after (hatched bars) 20 hours of restraint stress. Total tissue RNA was prepared and analyzed for TF mRNA expression level by quantitative RT-PCR. The data are represented as the means and SD (n = 8) in each age group, and the error bars represent interanimal variation. $^{*}P < .05$ in 24m versus 8w mice; $^{**}P < .04$ in 24m versus 8w mice; $^{***}P < .02$ in 12m versus 8w mice.

water, and counterstained with hematoxylin/eosin. No specific hybridization signal could be detected in parallel sections using ^{35}S-labeled sense probes in each experiment (not shown).

Preparation of antimouse TF antibody and Western blot analysis

Polyclonal rabbit antiserum specific for mouse TF (2 mg/mL, 1:2000 dilution in Tris (tris(hydroxymethyl)aminomethane)–buffered saline (TBS) containing 0.1% Tween-20 (TBS-T) was kindly provided by Drs K. Enjyoji and H. Kato, National Cardiovascular Center and Research Institute, Osaka, Japan. This specific antibody was raised in rabbits by the direct introduction of the encoding cDNA of mouse TF cloned into the pcDNA3 plasmid as described previously.[27,28] Serum titers and the specificity of the antibody were determined by standard Western blot analysis using protein extracts from COS-7 cells expressing mouse TF and recombinant mouse TF fused to glutathione-S-transferase protein (Amersham Pharmacia Biotech, Tokyo, Japan) (not shown). TF antigen in the lysates of adipose tissues obtained from obese and lean mice after 0, 2, and 20 hours of restraint stress was determined by sodium dodecylsulfate–polyacrylamide gel electrophoresis (SDS-PAGE) and Western blot analysis using the enhanced chemiluminescent (ECL) detection system (Amersham International, Buckinghamshire, United Kingdom). Briefly, each 2 μg of the tissue lysates was electrophoresed under reduced conditions on an 8% SDS-PAGE and transferred to polyvinylidene difluoride (PDVF) membranes (Bio-Rad Laboratories, Hercules, CA). The membranes were soaked in TBS containing 5% nonfat milk and 0.1% Tween-20 for 1 hour at room temperature to block additional protein binding sites and washed 3 times (15 minutes/wash) in TBS-T. The membranes were then incubated with antimouse TF, washed 4 times in TBS-T, and incubated for 1 hour with peroxidase-linked donkey antirabbit antibody (Amersham). After 3 washes in TBS-T, the membranes were developed with the ECL detection kit according to manufacturer's instructions.

Results

Induction of TF mRNA in tissues of the restraint-stressed mice

Initially, the effects of short and long exposure to restraint stress on the expression of TF mRNA in tissues were investigated in 8-week-old male C57BL/6J mice by using quantitative RT-PCR technique (Figure 1). Short duration (2 hours) of stress to mice did not substantially increase TF mRNA in all tissues examined. In contrast, a substantial induction of TF mRNA was detected in kidneys (6-fold), small intestines (2-fold), aortas (2-fold), and

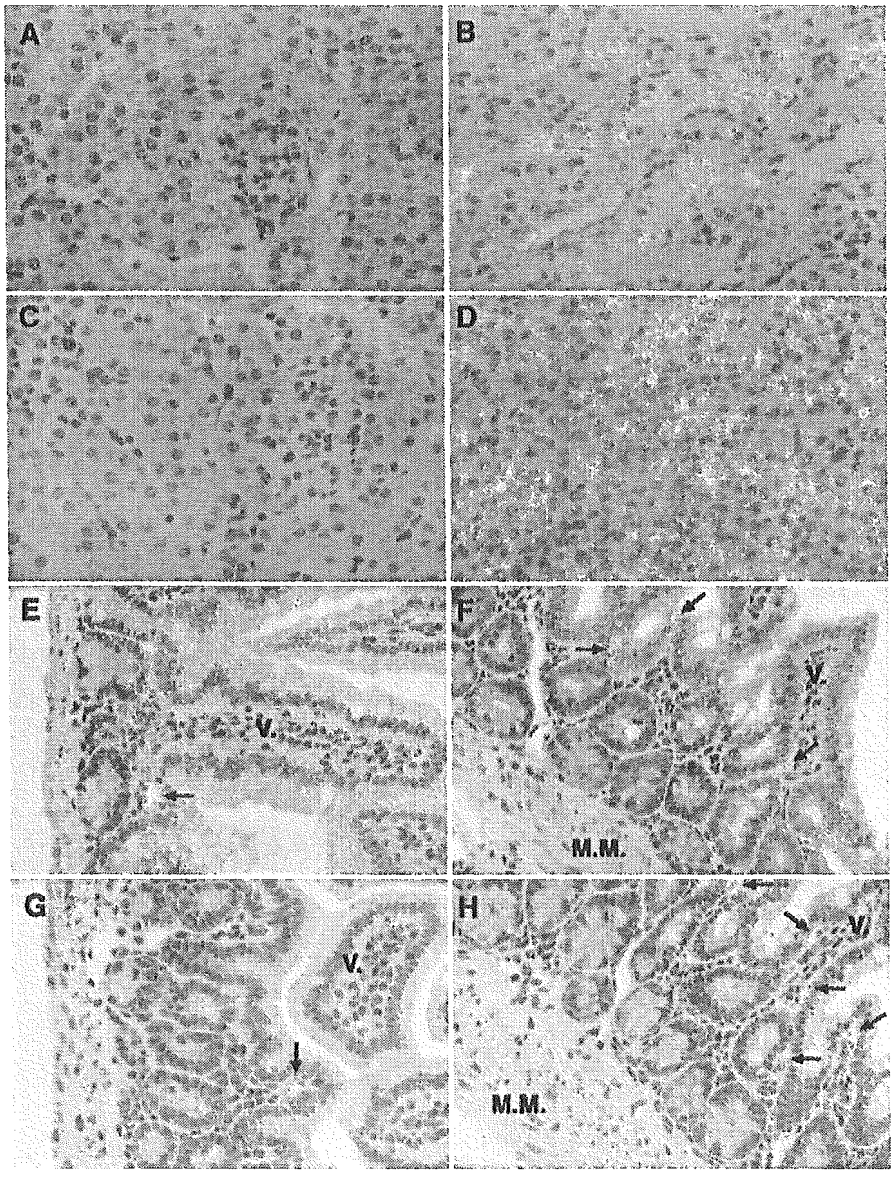

Figure 3. In situ hybridization analysis of TF mRNA in the kidneys and small intestines of control and stressed mice. Kidneys were harvested from 8-week-old and 12-month-old mice before and after 20 hours of restraint stress. Small intestines were also harvested from 8-week-old and 24-month-old mice before and after 20 hours of restraint stress. Both tissues were analyzed by in situ hybridization with the use of ^{35}S-labeled cRNA probes as described in "Materials and methods." The hybridization signal for TF mRNA corresponds to the light blue dots in panels B,D-H. (A-D) Kidneys of the unstressed (A, 8 weeks old; C, 12 months old) and stressed (B, 8 weeks old; D, 12 months old) mice. (E-H) Small intestines of the unstressed (E, 8 weeks old; G, 24 months old) and stressed (F, 8 weeks old; H, 24 months old) mice. Arrows indicate cells that are strongly positive for TF mRNA. M.M. indicates muscularis mucosae; V., villous core. All slides were exposed for 10 weeks at 4°C. Original magnification × 400.

adipose tissues (2-fold) after 20 hours of restraint stress. Unexpectedly, little or no responses of TF gene to restraint stress were observed in livers, lungs, hearts, and brains. These results suggest that the induction of TF gene by restraint stress occurred in a tissue-specific manner.

Stress-induced TF mRNA expression in young and aged mice

Experiments were performed to investigate the effect of aging on the induction of TF expression by restraint stress, using young (8-week-old) and extremely aged (12- and 24-month-old) mice (Figure 2). Basal (before stress) levels of TF mRNA expression in the tissues were slightly elevated in aged mice, but the differences were not substantial. Importantly, the magnitude of induction of TF mRNA expression in kidneys, small intestines, aortas, and adipose tissues substantially increased as animals age (Figure 2). Only in kidneys, TF mRNA expression was more increased by stress in 12-month-old mice than in 24-month-old mice. Again, no substantial induction of TF mRNA by 20 hours of restraint stress was observed in livers, lungs, hearts, and brains both in young and aged mice (not shown).

Cellular localization of TF mRNA in tissues of the restraint-stressed mice

To localize the TF mRNA induced by restraint stress in each tissue, in situ hybridization analysis was performed by using tissue sections from the control and stressed mice. Although there was no detectable signal for TF mRNA in kidneys of the unstressed aged mice (Figure 3 A,C), the epithelial cells of proximal and distal tubules (Figure 3B,D) in the stressed mice expressed abundant TF mRNA. Moreover, signals for TF mRNA in renal tubular epithelial cells were dramatic in the stressed aged mice compared with young mice (Figure 3B,D). In small intestines of the stressed mice, several cell types, including smooth muscle cells and inflammatory cells, in the villous core, in lamina propria, and in muscularis mucosae, showed strong signals for TF mRNA (Figure 3F,H) although these cells occasionally expressed TF mRNA in the unstressed mice (Figure 3E,G). Again, the increased signals for TF mRNA by stress in the intestinal cells were dramatic in aged mice (compare Figure 3F with 3H). These results are consistent with the data obtained by quantitative RT-PCR assay (Figure 2).

In aortas, only focal signals for TF mRNA were detected in the unstressed young and aged mice (Figure 4 A,C). However,

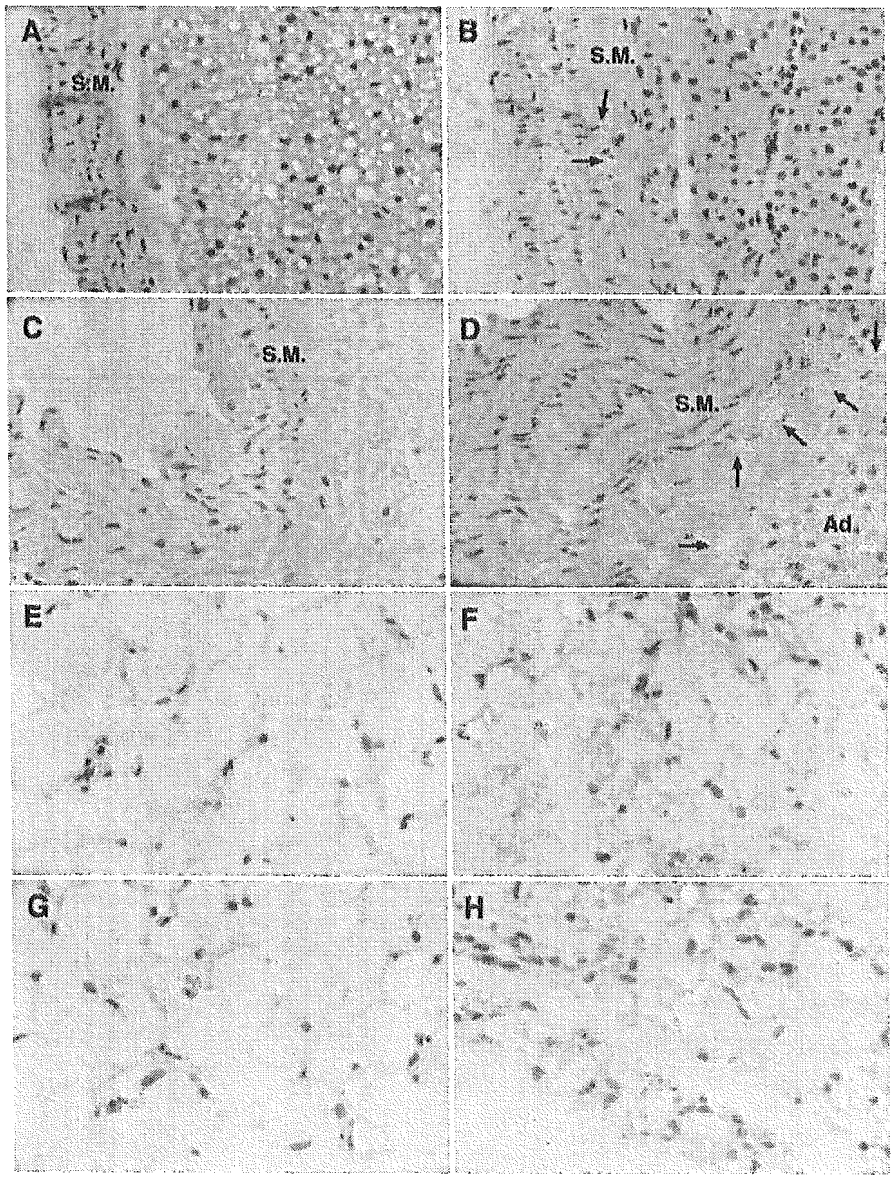

Figure 4. In situ hybridization analysis of TF mRNA in the aortas and adipose tissues of control and stressed mice. Aortas and epididymal fat tissues were harvested from 8-week-old and 24-month-old mice before and after 20 hours of continuous restraint stress and then analyzed by in situ hybridization as described in "Materials and methods." The hybridization signal for TF mRNA corresponds to the light blue dots in all panels: (A-D) Aortas of the unstressed (A, 8 weeks old; C, 12 months old) and stressed (B, 8 weeks old; D, 12 months old) mice. Arrows indicate cells that are strongly positive for TF mRNA in the adventitia of aorta. S.M. indicates vascular smooth muscle layer; Ad, adipose tissue around the vessel wall of aorta. (E-H) Epididymal fat tissues of the unstressed (E, 8 weeks old; G, 24 months old) and stressed (F, 8 weeks old; H, 24 months old) mice. All slides were exposed for 10 weeks at 4°C. Original magnification for all panels × 400.